Replies to the Associate Editor (Christof Janssen)

We would like to thank the editor for his thorough comments/suggestions. Below are the replies to his questions and the modifications we added to the manuscript. The editor's comments are highlighted in red font while our replies are in black font.

Comments to the Author:
Dear authors, I congratulate you to your very interesting work that the referees have attested to be scientifically sound. Thank you also for responding to their requests in detail. I have thoroughly reread the revised manuscript and there is still a (long) list of minor corrections that should be addressed before publication (see further below). There are also four important issues that should be adressed in a further revision process:

P10 L227-228 In the case of CO2, the dilution of oxygen due to 400 ppm of CO2 is significant, and larger than any direct spectral interference.

I don't think you give detailed information (in form of an equation) on how the analyzer obtains its result from the measured quantities. The CRDS methd (and you could recall the fundamental equation) provides direct access to the particle number density of O2 (knowing the spectral data). How is the mixing ratio X_O2 obtained ? In principle you could use p and T, but I think this is not precise enough and some calibration is employed. Please give an equation or a reference where one sees how measured quantities (after correction or not) give O2 mixing ratios. (This would also allow to understand where the dilution effect comes from). The same holds for the conversion into O2/N2: what is the assumption on N2 (or f_N2) made in your algorithm to convert from X_O2 to O2/N2. What are the roles of water and CO2 ? Your data show that this is crucial information that is yet missing. Since your paper is the first description of such a system, the information must be provided.

The relationship of the measured quantities to the reported result is described very explicitly in lines 308—312 of the MS. As the reviewer mentions, the number density is directly proportional to the optical absorption, and for controlled temperature and pressure the number density is proportional to the mole fraction. It is correct that we cannot measure temperature and pressure to the permeg level, hence calibration is required and this is actually the heart of the paper. We know that there are dilution effects from CO2 and water. Water can be removed by drying but since we have no way to measure CO2, any dilution correction has to come from an independent measurement. Unlike mass spectrometry, we do not measure O2/N2 directly; it can only be inferred by calibrating with standards. None of this should be remarkable – the same considerations apply to any optical method, whether it is diamagnetism or refractive index or absorption or whatever. The key is a quantitative measure of oxygen concentration that is precise, stable, and calibratable at the permeg level.

P21 L500++

Based on the evidence that you provide in this paragraph you should consider writing "The most likely cause for the drift is the optical amplifier ..." or "We believe that the optical amplifier has caused the drift ... instead of "A possible hypothesis for the cause of the drift can be an optical emplifier ..."

In line 504, we have now modified the sentence as:

“We believe that the optical amplifier has caused the drift in the first system…”

P21 L491++

The section describes tests of the systems' water correction function.
You should consider organisation/presentation of this paragraph. If I strongly summarize and exaggerate this paragraph, then the water correction works if there is no water and it does not if there is water in the samples.

This section is now reorganized and modified mainly in the paragraph below:

Figure 15a shows the dried ambient air water measurements in both analyzers with frequent spikes due to valve switching while measuring standard gases. In the second case, where the water trap was by-passed and non-dried air was allowed to the CRDS analyzer keeping the dried air flow to the NDIR (Figure 15b), a clear increase in the water measurements in the CRDS analyzer can be observed. Here, it should be noted that there are no spikes in the water measurements of the CRDS analyzers as there are no standard gas measurements in between and the inlet is directly connected to the CRDS analyzer (Figure 11). Figures 15c & 15d show the difference in oxygen measurements of ambient air measured in both analyzers in the two cases stated above (note that the CRDS uses its built-in water correction function applying Eq. 5).

Figures/units

Please use a consistent notation to indicate units in axis labels. Most of the time units are given in parantheses, but some figures use brackets (Figs. 2, 5, 8, 9, 10), some use a slash (Fig. 7), some don't use anything at all (Fig. 17), and some even mix brackets and parantheses (Fig. 1).

These comments are now addressed as pointed out here with all the units in Parenthesis

List of detailed suggestions/corrections

P1 L16-17: Change to : Here we present a detailed description ...

The missing “a” is now added

P2 L35-40: Please check grammar, also consider that the choice of the unit (per meg) and the choice of the measurement quantity (O2/N2) are two different things. It would be better first to introduce the quantity O2/N2 and explain why and then the corresponding unit (small relative deviation from a standard).

As the editor´s suggestion we have now added the following paragraph and modify this section:

Measurements of atmospheric O2 are reported as the ratio to the N2 concentration and expressed as δ(O2/N2) because the variations in the concentrations of other atmospheric gases such as CO2 can influence the O2 partial pressure while this ratio is insensitive to these changes in other gases. These variations in atmospheric O2 is commonly expressed in units of per meg due to its small variations with respect to a large background, where

$$\delta\left(\frac{O_2}{N_2}\right)(per\ meg) = \left(\frac{(\frac{O_2}{N_2})_{sample}}{(\frac{O_2}{N_2})_{reference}} - 1\right).10^6$$

P2 L40+ Please give a conversion formula that converts between the different units per meg and ppm (could be in the appendix). This would enable to better understand your results (eg. correlation plots in appendix).

We convert per meg to parts per million equivalent by multiplying per meg by 0.209500 (the O2 mole fraction of atmospheric air)

P3 L49-53: One gets confused about alphas and ORs in this paragraph. Please define. Use comma after OR. What is alpha ? Has it been defined before ?

This section is now rephrased to include OR and alpha definition as:

This method hinges on the linear coupling between CO2 and O2 with an oxidation ratio (OR, defined as the stoichiometric ratio of exchange during various process such as photosynthesis and respiration expressed using α) of 1.1 for the terrestrial biosphere photosynthesis-respiration processes (αb) and 1.4 for fossil fuel combustion (αf) while they are decoupled for oceanic processes (αo = 0).

P3 L52: give alpha_ocean for the decoupled process (alpha_o = 0)

See above

P3 L59: ... several, mostly custom built techniques ...

Corrected accordingly as ... several, mostly custom built techniques ...

P3 L69: monitoring(Note -> monitoring (note

Small n is now used

P4 L87: If you capitalize for mentioning the acronym of a DFB laser, please also capitalize the B in feedback

B is now capitalized

P5 L96-98: A drawing of the optical setup is missing. Please state briefly how the wavelength monitor is integrated in the optics (beam splitter, ...).

The following paragraph is now added:

“The wavelength monitor is a fiber-coupled device located between the laser and the cavity. A fraction of the beam from the input fiber is collected using a beam splitter for the measurement wavelength and the remaining power is collected in the output fiber.”

P5 L98: It is a little bit strange to read : "the data acquisition system sweeps the laser frequency ...".

This sentence is now modified as:

“The instrument´s data acquisition system is used to sweep the laser frequency….”

P6 L100 (P9 L 198, 202): Strictly speaking, 7878.805547 cm-1 is no frequency, remove "a frequency of"

Removed “…a frequency of…” at these lines

P10 L221-224: It is not clear what you want say here. The H2O line clearly needs to be considered even if its line strength is only 10 to 20 % of the O2 line.

We do consider interference from water, as the text clearly states. The point of ll. 221-224 is that we do not have to worry about deuterated water interfering with the O2 measurement because these lines are well separated.

P10 L217-228: There seems to be little advantage in using AFGL notation. General understanding would greatly benefit from dropping this notation and call isotopologues by their names: water and deuterated water or by their isotope formula ^1H_2^16O etc.

The AFGL notation is useful because of its conciseness and for clarity we have provided a clear definition of these on lines 237-239 as:

“The main features are the Q13Q13 line from trace contamination of oxygen in the sample and several lines that arise from normal water ($^{1}H_{2}{}^{16}O$, AFGL code 161) and deuterated water ($^{1}H^{2}H^{16}O$, AFGL code 162, also abbreviated HDO).”

P10 L218: I could not find traces of the heavy water isotopologues in the lower panel of Fig. 5. It seems that the figure has not been updated in the revised version, contrary to what has been indicated in the response to the reviewers. The caption also lacks the update.

The correct figure is now provided as shown below.

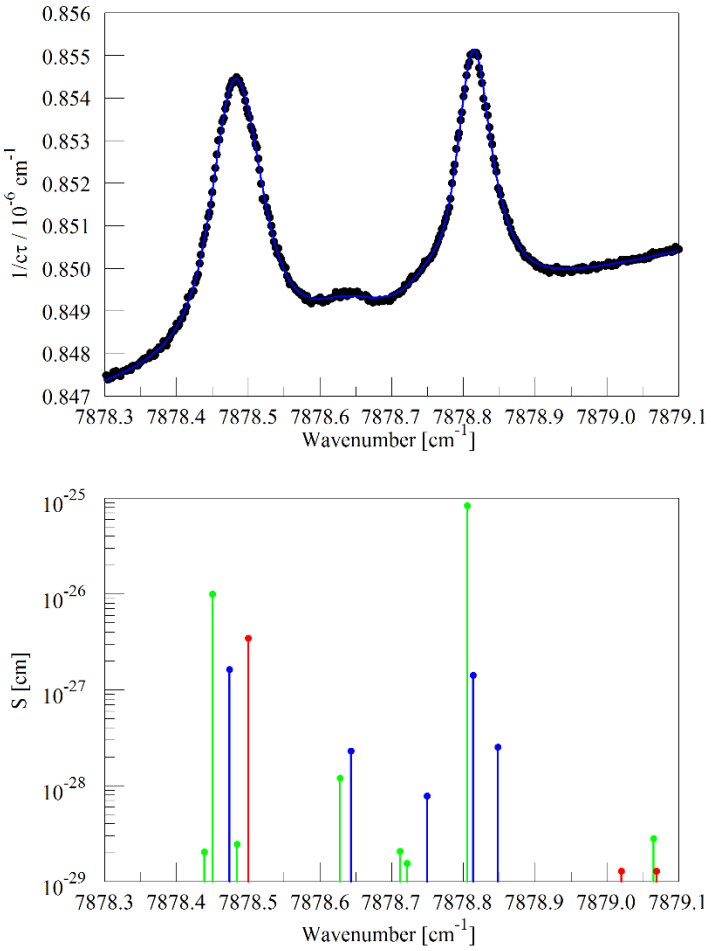

Figure 5. Upper panel: spectrum of water in nitrogen (points) and fit to Voigt model (blue curve). Lower panel: Oxygen (green), normal water (blue), and deuterated water (red) lines in the 2016 Hitran data base.

P10 L236: AFGL abbreviation -> AFGL code; please see remarks in the beginning.

See above

P11 L255-259: The description is misleading, because line profiles (area = 1) are not multiplied by amplitude, but by the line strength. Please phrase differently. Also what are the weak perturbing peaks ?

This comment is a bit unclear this sentence states exactly the procedure that was used. Our line profiles (which are not defined the same way as Hitran's, but are very explicitly explained in ll. 236-238) and our amplitudes are self-consistent. We specifically use the word "amplitude" and not "line strength" because we are describing our fitting procedure and not a Hitran calculation.

However, we modified the section "three water peaks and the two weak perturbing peaks" as

“the water spectrum is modeled with three peaks: one strong line and two weak perturbers”, as described in lines 198-202 on p. 9.

P11 L260: I don't understand the phrase "that constrained to be in fixed ratios to be in fixed ratios". Is there a "were" missing ? "ratio" should probably be replaced by "proportion".

Corrected by adding “were constrained” and “ratio” is replaced by “proportion” (lines 263-264)

P12 L259-260: You might look up the recent HITRAN update.

This comment is a bit unclear. We used Gordon et al. 2017 for referring to the HITRAN in this MS and we will be glad to know if there is any update that is important and we are not aware to include in this section.

P12 L263: Please use here and at other instances the notation Filges et al. (2018) and not Filges et al. (Filges et al., 2018) when citing the author in the text.

Now corrected as Filges et al. (2018)

P12 L252: The water lines ... change , into ; before rather.

Changed to “rather;…”

P15 L322-324: check passive voice in "there is no advantage to be obtained" and the whole phrase. It does not sound correct.

In line 343, we have now modified this phrase as:

“One is that in determining an isotopic ratio, normalizing absorption amplitudes to line widths does not provide any advantage, instead we simply take the ratio of amplitudes to compute delta.”

P15 L346: Giving the absolute value of 5e-9 cm-1 does not help in the argument. 1. there are CRDS systems that measure lower absorptions. 2. You don't give an equivalent value for an absorption that is easily measurable (such as the 16O16O isotopologue).

Our statement is valid as stands – signal-to-noise is not adequate to measure amplitude and width independently.

As to point 2, the absorption of the 16O16O isotopologue is clearly shown in Figure 1.

P15 L333: Is much less precise: It should be sqrt(305/40) ~ 3 times less precise. Is this much less precise ?

The line intensity for the 16O16O measurement is also less for the isotopic mode than for the concentration mode, which makes the precision even worse than the factor of 3 computed above. The isotopic mode was not intended to give precise mole fraction.

P15 L337-339: The phrase "One set of tests aimed at determining the impact of pressure or temperature drifts or of uncobtrolled noise on the concentration measurements" ? can be much simplified to ease reading. What is uncontrolled noise ? This needs to be clarified.

We have now removed the word “uncontrolled” in line 362.

P15 L353: Drift -> drift

Corrected as drift

P15 L356: insolated ?

It is now corrected as “insulated”

P15 L358: regulator -> pressure regulator

Added “pressure regulator”

P16 L358-360: and reducing the flow ... -> and with an additional orifice to reduce the flow to about 55 sccm.

Now corrected by removing “and reducing the flow”

P16 L369: Use the term "Allan-Werle plot" in combination with Allan variance

We now used “Allan-Werle plot”

P16 L372: Define tau

We now defined Tau as “Tau is the abscissa of an Allan-Werle plot”.

P16 L377: times scale - time scales

Time scales is now used

P17 L384: available Oxzilla fuel cell -> available fuel cell

The name “Oxzilla” is now removed

P17 L389: flow was adjusted to. It might be preferrable to use sccm as well.

Corrected as “Flow from each …”

P17 L391: flow out of the Oxzilla was ... -> flow out of the fuel cell analyzer was

Corrected as “..flow out of the fuel cell analyzer…”

P17 L389++ : The use of different flow units is confusing. Please stick to sccm.

We now used sccm

P17 L397: It should be LabView instead of Lab VIEW. Could you specify the reason for using a labview program or is this not interesting ? Then drop this detail.

Corrected to “LabView”

P17 L398: I know "a priori", but what does "in priori" mean ? A priori wouldn't make no sense here, however.

We now used “First” instead of “In priori”
P19 L447+: "While similar correlation coefficients were observed for both analyzers, different slopes were calculated (Fig. A.1). This is due to the fact that the IRMS measures the O2 to N2 ratio (δ(O2/N2)) in per meg, while the CRDS and the Paramagnetic analyzers provide non-calibrated O2 mixing ratios in units of ppm and per meg, respectively." Is this true ? I cannot come up with the observed slope values when I try to use the definition of per meg and ppm.

As we stated the difference is due to two reasons:

- Conversion factor between ppm and per meg
- Uncalibrated results from the Paramagnetic analyzer

So using only a conversion factor will not reproduce the observed slopes.
P18 L425: fractions -> mole fractions (change here and elsewhere)

Corrected as mole fractions

P18 L426: change and to or in "very low and very high O2".

Changed to “or”
P18 L426: standard 6 and 7 -> standards 6 and 7

Changed to standards 6 and 7

P18 L427: standard 7 was not measured on the IRMS ... change O2 mixing ratios to singular

Changed to “…the O2 mixing ratio is unknown”

P18 L429: between -> measured with

Corrected to …measured with…
P19 L432: lower in O2 -> lower

P20 L471: accounted -> accounted for

Corrected in line 501 now

P20 L474: in similar pattern -> following similar patterns

Corrected as suggested

P20 L477: The phrase repeats what has been said before. You could write. Interestingly the drift pattern could be modeled ...

Now modified as:

“Interestingly, the drift pattern can be modeled using a polynomial function which can…”

P20 L475: repeated use of drift. Drop the first in the sentence

Modified as “..Interestingly, this p[attern….”

P22 L506: Based on these plots -> Based on this plot

Now modified as “Based on this plot…”

P22 L506: I think that the essential features are reproduced but I don't think that there is very good agreement. Eg the NDIR shows an exponential response time when the CRDS is not.

We partly agree with the editor’s reasoning, yet we have to bear in mind that we are talking water amounts in the very low ppm range. For these two analyzers that is the limit of their capabilities. Therefore, it was astonishing that the behavior is very similar with only very few exceptions. We would like to keep our statement since it also states the fact that we deal with low water contents.

P22 L509: measured in, not measured into

Deleted “to”

P22 L509 & P47 F15: The signals in panels a and b need to be explained. Where do the spikes come from and why does . Without such explanation it is impossible to follow your argument whether the agreement is good or not.

This is now included to the comments of Figure 15 below and in lines 540-549 in the manuscript.
P22 L512: in-built -> built-in

Corrected

P23 L545: "embedded within", check grammar

Now changed to “…installed inside..”

P24 L549: a low span -> low span ....

Corrected as low span

P24 L554+: Check phrase

It is now modified as:

“Despite the strong variability, …”

P25 L555: It might be interesting to know which of the two devices was the first in the series.

Similar to the setup in Figure 11, the Paramagnetic system was first in the series.

P27 L634: no CO2 possible interference from band overlap -> it has no interference from a possible overlapping absorption from a CO2 band.

Now it is modified as “…as it has not interference from possible CO2 absorption band overlap”.

P28 L659: delete "if it appears"

Deleted “if it appears”

P29 L677: "However" does not make a sense here.

Deleted “However”

P29 L680: What is "about a significant decrease" ?

Deleted “about” and the sentence is now read as:

“..we have observed a significant decrease in precision (about ten-fold) in…”

P29 L684: This conclusion is not identical to what is presented in the results section, where CO2 and CO are excluded.

This sentence is not contradicting the results section as it simply explains the components of breath air (CO_2, CO, CH_4 and O_2). For clarity we removed the line “… as breath air contains CO_2, CH_4 and CO in addition to oxygen.” And the sentence is modified as:

“However, such measurements for a breath air showed a contrasting signal, possibly due to interference from other gases such as CH4.”

P40 F8 : C -> °C

Figure 8 is now updated as follows:

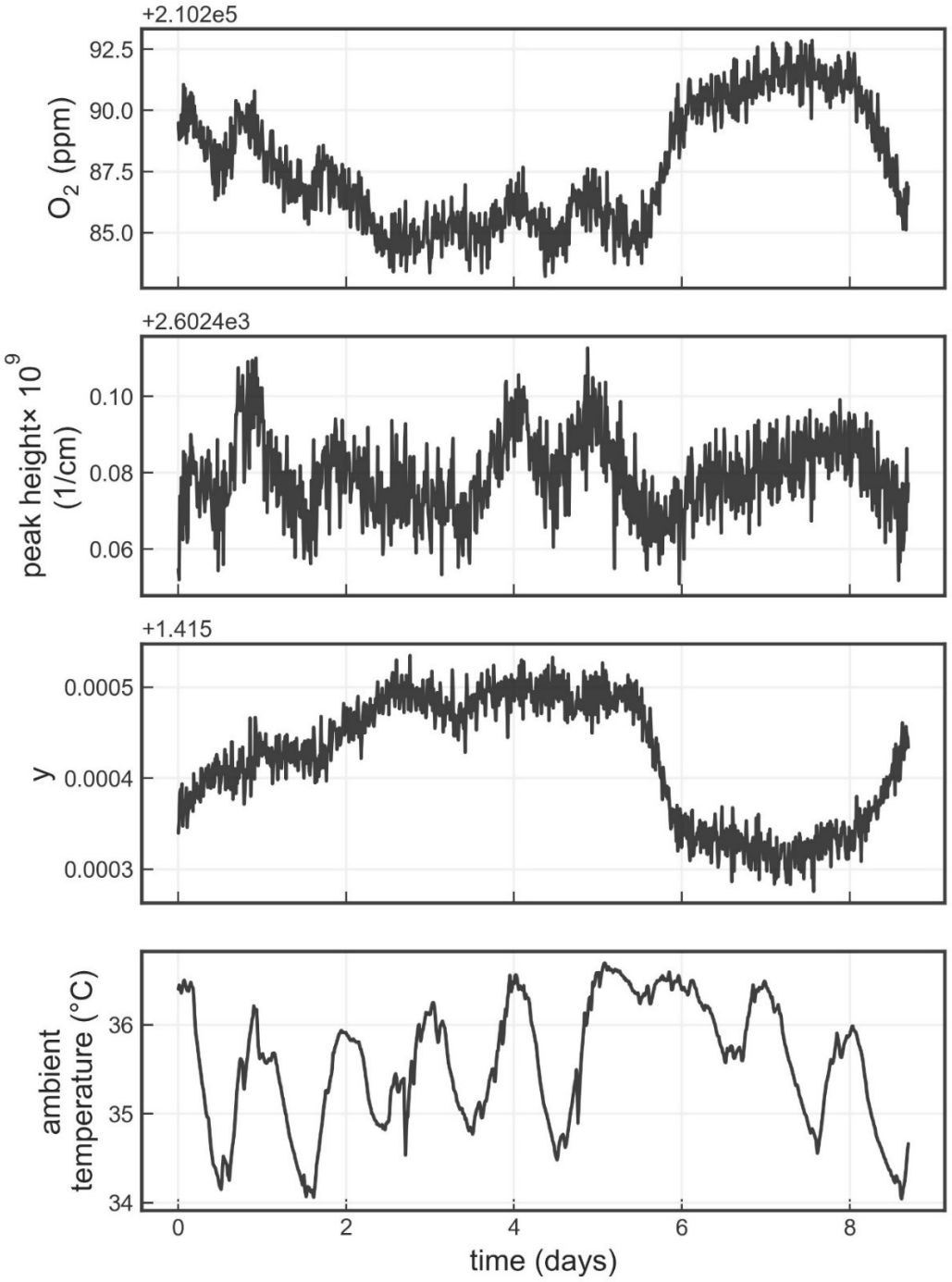

P40 F8 : upitalic O2 -> upright O2

See above

P41 F9 : mention tau in legend (otherwise it is undefined in the figure caption)

Already explained in the main text as requested above

P46 F14: Please increase the size of the labels for CRDS and NDIR in the figure for readability
We have now modified this figure as follows

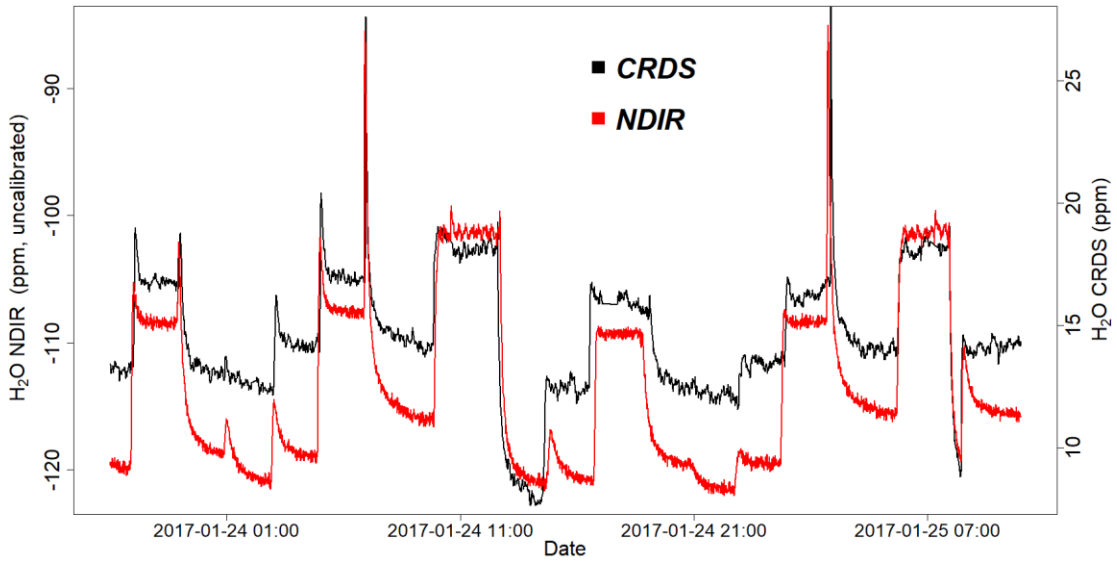

Figure 14. Parallel water vapor measurements for a dried ambient air by both the NDIR and CRDS analyzers. Note that the water values from the NDIR analyzer are not calibrated.

P46 F14+ later on. SI units for mole fractions are mmol/mol, µmol/mol etc. The atmospheric community often uses permil, ppm etc for the same purpose. It would be better to be coherent and convert the NDIR water data to ppm, if this is the preferred (non-SI) unit of the authors. Using different units for the same quantity is confusing. The offset of the NDIR data is worrysome as it implies negativ values, which are physically impossible.

It is now converted into ppm.

The negative offsets in the NDIR are due to the uncalibrated water values as explained in the main text and Figure legend.
P46 F14: please shortly mention the reason why the NDIR analyzer always seems to relax into the stable O2 value after a humidity change whereas the CRDS does this only in a few cases.

This question is not clear plus the Figure does not display any O2 data.

P47 F15 : Please shortly explain origin of spikes in panels a and b.

These are standard gases measured in between samples and the spikes are due to valve switching.

P48 F16 : It would probably be interesting to have a histogram plot of the lower panel or a line fit (slope = 0 or different) to these data.

A horizontal line with slope of zero is now added.

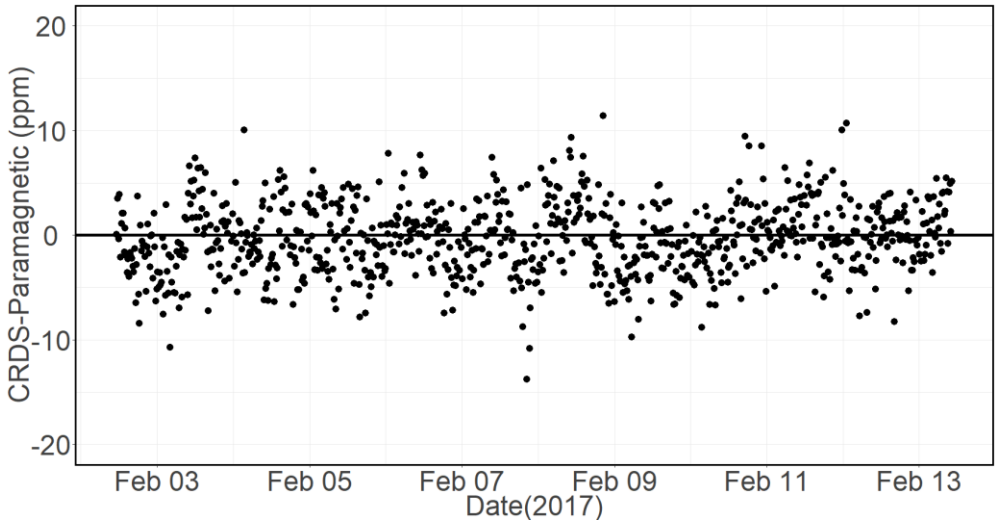

P49 F17 : Figure is not in publishable quality. Axis labels on left hand side are cut. Also adapt label font to y- axis font (bold) and put units in parantheses.

This figure is now modified as shown below.

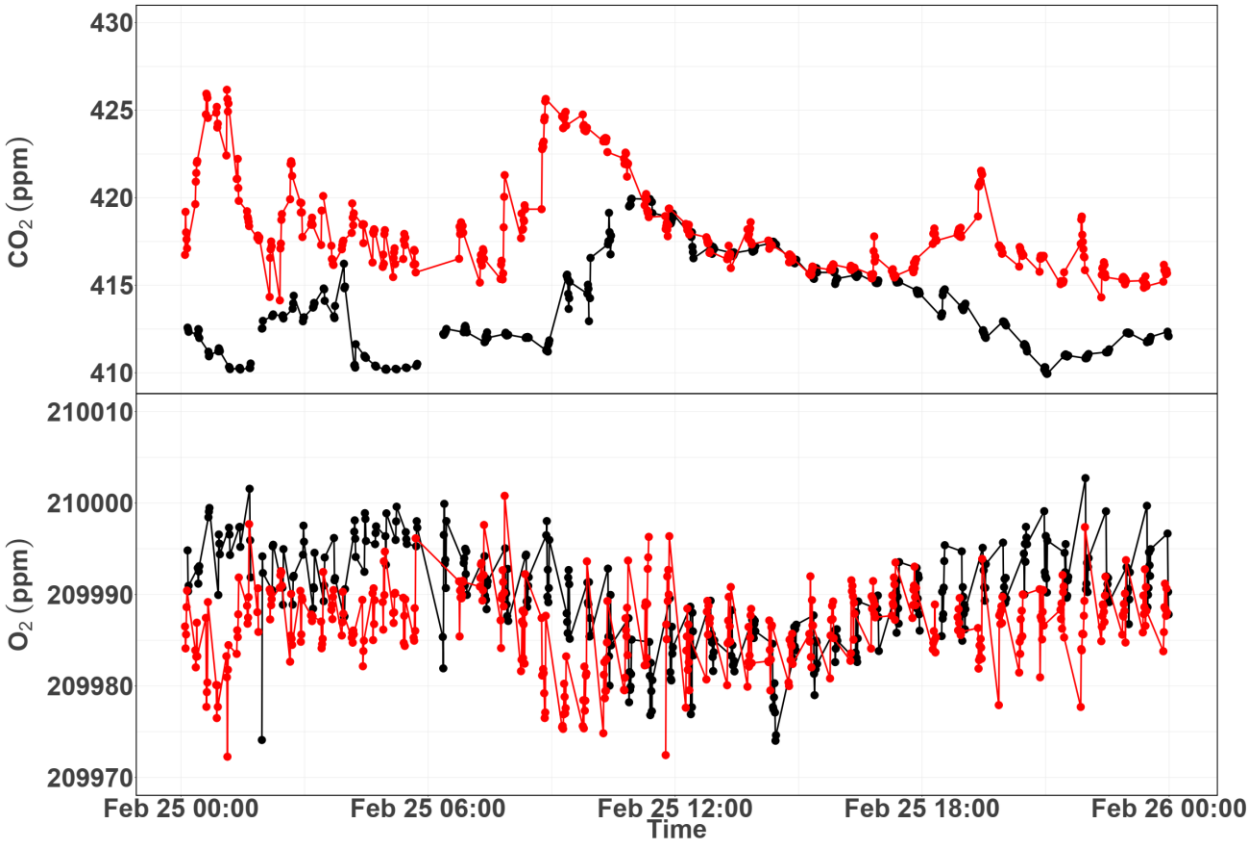

Figure 17. Diurnal variations of CO_2 (top) and O_2 (bottom) measurements from the 12 m (red) and the 212.5 m (black) height levels at Beromünster tower.

P50 F18 : Time scales of the two time series are different. Please align upper trace on the scale of the lower trace.

The figure is now adjusted as follows

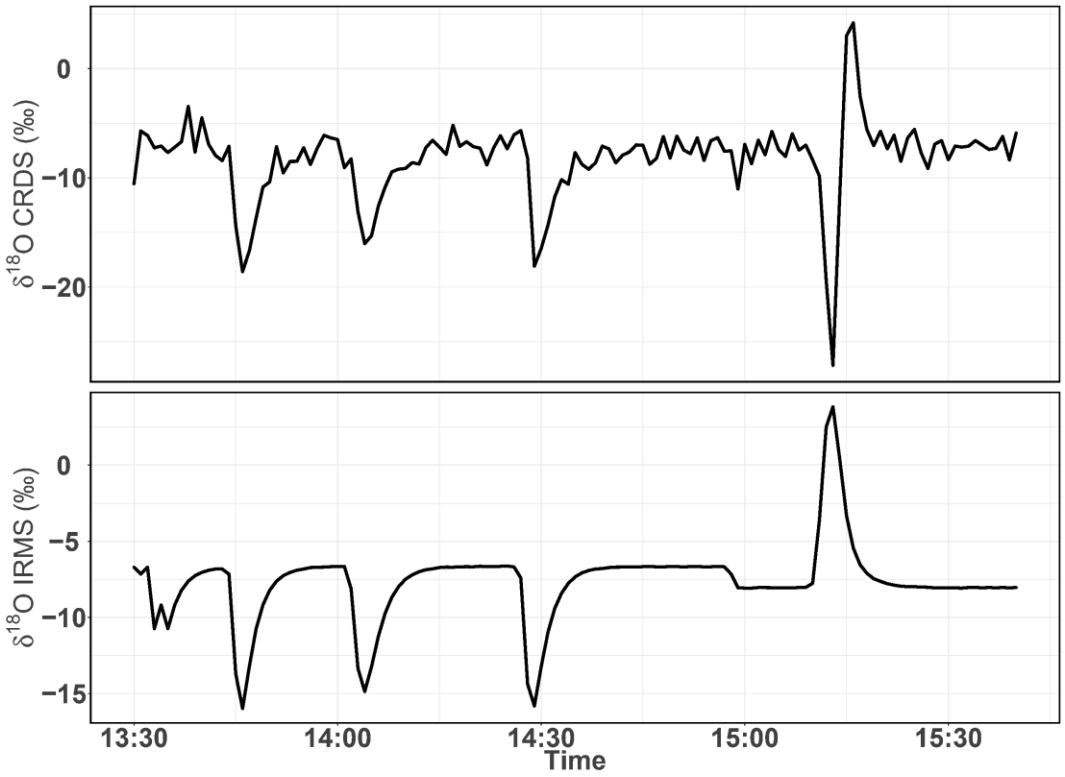

P51 FA.1: Change "zooming only to standards 1-5" -> "selecting standards 1-5"

Changed to “selecting”

P51 FA.1: Convert all quantities into same units so that deviations from 1:1 correspondances can be spotted easily.

We kept these measurements in their respective units purposely, in case the reader is interested in converting the measured values in the multiple figures in this manuscript and to check any agreement/difference among these three analyzers. If we change the units, it will be difficult for the reader to easily check how we interconvert and compare the different results in the different plots.

P51 L910: Please change section title into something more specific. It is presently not very informative.

Removed the tittle “Additional plots”

High-precision atmospheric oxygen measurement comparisons between a newly built CRDS analyzer and existing measurement techniques

Tesfaye A. Berhanu[1,2], John Hoffnagle[2], Chris Rella[2], David Kimhak[2], Peter Nyfeler[1], Markus Leuenberger[1]

[1]*Climate and Environmental Physics, Physics Institute and Oeschger Centre for Climate Change Research, University of Bern, Bern, Switzerland*

[2]*Picarro Inc., 3105 Patrick Henry Drive, Santa Clara, CA, USA*

Abstract

Carbon dioxide and oxygen are tightly coupled in land-biospheres CO_2 - O_2 exchange processes, while they are not coupled in oceanic exchange. For this reason, atmospheric oxygen measurements can be used to constrain the global carbon cycle, especially oceanic uptake. However, accurately quantifying the small (~1-100 ppm) variations in O_2 is analytically challenging due to the very large atmospheric background which constitutes about 20.9 % (~209500 ppm) of atmospheric air. Here we present a detailed description of the analyzer and its operating principles as well as comprehensive laboratory and field studies for a newly developed high-precision oxygen mixing ratio and isotopic composition analyzer (Picarro G-2207) that is based on cavity ring-down spectroscopy (CRDS). From the laboratory tests, we have calculated a short-term precision (standard error of one-minute O_2 mixing ratio measurements) of < 1 ppm for this analyzer based on measurements of eight standard gases analyzed for two hours consecutively. In contrast to the currently existing techniques, the instrument has an excellent long-term stability and therefore a calibration every 12 hours is sufficient to get an overall uncertainty of < 5 ppm. Measurements of

Formatted: Subscript

ambient air were also conducted at the High-Altitude Research Station, Jungfraujoch and the Beromünster tall tower in Switzerland. At both sites, we observed opposing and diurnally varying CO_2 and O_2 profiles due to different processes such as combustion, photosynthesis and respiration. Based on the combined measurements at Beromünster tower, we determined height dependent O_2:CO_2 oxidation ratios varying between -0.98 to -1.60 , which increase with the height of the tower inlet, possibly due to different source contribution such as natural gas combustion with high oxidation ratio and biological processes which are at the lower end.

1. Introduction

Atmospheric oxygen comprises about 20.9 % of the global atmosphere and in the past decade its concentration decreased at a rate of ~ 20 per meg yr-1 (Keeling and Manning, 2014) mainly associated with the increase in fossil fuel combustion. Measurements of atmospheric O_2 are reported as the ratio to the N_2 concentration and expressed as $\delta(O_2/N_2)$ because the variations in the concentrations of other atmospheric gases such as CO_2 can influence the O_2 partial pressure while this ratio is insensitive to these changes in other gases. These variations in atmospheric O_2 is commonly expressed in units of per meg due to its small variations with respect to a large background, where

~~$$\left(\frac{O_2}{N_2}\right)(per\ meg) = \left(\frac{(\frac{O_2}{N_2})_{reference}}{(\frac{O_2}{N_2})_{sample}} - 1\right).10^6$$~~

$$\delta\left(\frac{O_2}{N_2}\right)(per\ meg) = \left(\frac{(\frac{O_2}{N_2})_{sample}}{(\frac{O_2}{N_2})_{reference}} - 1\right).10^6 \quad (1)$$

Note that we convert per meg to parts per million equivalent by multiplying per meg by 0.209500 (the O_2 mole fraction of atmospheric air).

In contrast to O_2, the global average atmospheric CO_2 mixing ratio increased to ~~402~~405.~~8~~0 ppm averaged over ~~2016~~2017 ~~(predicted to grow by 2 % in 2017)~~ since its preindustrial value

Formatted: Left, Indent: First line: 0", Space After: 10 pt

Formatted: Subscript

Formatted: Subscript

Formatted: Subscript

Formatted: Subscript

Formatted: Subscript

Formatted: Subscript

of 280 ppm (Le Quéré et al., 2017). As the variability of atmospheric oxygen is directly linked to the carbon cycle, both its short and long-term observations can be used to better constrain the carbon cycle. For example, since first suggested by Keeling and Shertz (1992) the long-term trends derived from concurrent measurements of atmospheric CO_2 and O_2 have been widely used to quantify the partitioning of atmospheric CO_2 between the land-biosphere and oceanic sinks (Battle et al., 2000; Goto et al., 2017; Manning and Keeling, 2006; Valentino et al., 2008). This method hinges on the linear coupling between CO_2 and O_2 with an oxidation ratio (OR, defined as the stoichiometric ratio of exchange during various process such as photosynthesis and respiration expressed using α) of 1.1 for the terrestrial biosphere photosynthesis-respiration processes (α_b) and 1.4 for fossil fuel combustion (α_f) while they are decoupled for oceanic processes ($\alpha_o = 0$). Meanwhile, the short-term variability in atmospheric oxygen can be used to estimate marine biological productivity and air-sea gas exchange (Keeling et al., 1998; Nevison et al., 2012). However, the accuracy of these estimates is primarily linked to the accuracy and precision of atmospheric O_2 measurements and the assumed ORs for the different processes which are highly variable in contrast to atmospheric CO_2 that can be well measured within the precision guidelines set by the Global Atmospheric Watch (GAW) (± 0.1 ppm for the northern hemisphere).

Currently there are several, ~~techniques~~ mostly custom built techniques that can measure atmospheric O_2 variations as oxygen concentration based on interferometric, paramagnetic, UV absorption and fuel cell technology (Keeling, 1988a; Manning et al., 1999; Stephens et al., 2007) or as O_2/N_2 ratios to account for the large background effect using g~~G~~as chromatography with thermal conductivity detector (GC-TCD) or ~~Gas~~ gas chromatography coupled to mass spectrometry (GC-MS) (Bender et al., 1994; Tohjima, 2000). Despite the fact that these techniques have been ~~commercially available~~ used for more than two decades,

Formatted: Highlight
Formatted: Highlight
Formatted: Not Superscript/ Subscript
Formatted: English (United States)
Formatted: English (United States)

accurate quantification of atmospheric oxygen variability remains challenging primarily because the small ppm-level atmospheric oxygen signal rides on a ~ 210,000 ppm background, which places stringent requirements on the precision and drift of the analysis methods especially for continuous monitoring. (note that the GAW recommendation for the measurement precision of O_2/N_2 is 2 per meg). The techniques listed above struggle to routinely achieve the necessary performance for various reasons, including i) instability over time that requires frequent measurement interruption for calibration, ii) measurement bias with ambient and sample temperature and/or pressure, and/or iii) systematic errors in the measurement due to other atmospheric species. Further, some techniques require the use of consumables and rely on high vacuum, which complicates field deployment.

In this manuscript we describe a new high precision oxygen concentration and isotopic composition analyzer by Picarro Inc., Santa Clara, USA (G-2207) based on CRDS technology. Here, we will introduce the analyzer design principles in details, describe the unique features of the analyzer and evaluate its performance based on various independent laboratory and field tests by comparing it with currently existing techniques. Then, we will present and interpret our observations based on field measurements. Finally, we will conclude its overall performance and provide recommendations and possible improvements.

2. Analyzer design principles

The analyzer described here is derived from the Picarro G2000 series of CRDS analyzers. The basic elements have been described elsewhere (Crosson, 2008; Martin et al., 2016; Steig et al., 2014): briefly, the instrument is built around a high-finesse, traveling-wave optical cavity, which is coupled to either of two single-frequency Distributed FBFeedBack-stabilized semiconductor lasers. One cavity mirror is mounted on a piezoelectric translator (PZT) to allow fine tuning of the cavity resonance frequencies. A semiconductor optical

amplifier between the laser sources and the cavity boosts the laser power and serves as a fast-optical switch. The cavity body is constructed of invar and enclosed in a temperature stabilized box (T = 45° C, stabilized to approximately 0.01 °C) for dimensional and spectroscopic stability. A vacuum pump pulls the gas to be sampled through the cavity and a proportional valve between the cavity and the pump maintains the sample pressure in the cavity at a value of 340 hPa, with variations on the order of 1 Pa. The instrument has a wavelength monitor, based upon measurements of interference fringes from a solid etalon, which is used to control the laser wavelength by adjusting the laser temperature and current. The wavelength monitor is a fiber-coupled device located between the laser and the cavity. A fraction of the beam from the input fiber is collected using a beam splitter for the measurement wavelength and the remaining power is collected in the output fiber. A high-speed photodiode monitors the optical power emerging from the cavity. The instrument's data acquisition system is used to sweeps the laser frequency over the spectral feature to be measured, modulates the laser output to initiate ring-downs, and fits the ring-down signal to an exponential function to generate a spectrogram of optical loss versus laser frequency. For this instrument the empty cavity ring-down time constant is about 39 μs. Subsequent program modules compare the measured loss spectrum to a spectral model, using non-linear least-squares fitting (Press et al., 1986) to find the best-fit model parameters and thereby obtain a quantitative measure of the absorption due to the target molecule, and finally apply a calibration factor to the optical absorption to deduce the molecular concentration. When operating in its normal gas analysis mode, the instrument acquires about 200-300 ring-downs per second and achieves a noise equivalent absorption of typically about 10^{-11} cm^{-1} $Hz^{-1/2}$, with some variation between instruments.

Formatted: English (United States)

Formatted: English (United States)

The primary goal when designing this analyzer was to measure the molecular oxygen concentration with few-per-meg level precision and stability. In this context operational stability is as important as signal-to-noise. Our experience has been that the most stable operation of the analyzer is achieved when the optical phase length of the cavity is held as nearly constant as possible. In this case the free spectral range (FSR, 0.0206 cm^{-1}) of the temperature stabilized, invar ring-down cavity provides a better optical frequency standard than the etalon-based wavelength monitor, which in turn allows more consistent measurements of absorption line width and integrated absorption line intensity (Steig et al., 2014). For a small, field-deployable instrument, it is not practical to stabilize the absolute frequencies of the cavity modes to an optical frequency standard (Hodges et al., 2004) but the oxygen lines themselves, under conditions of constant temperature and pressure, provide an adequate frequency reference. The oxygen spectrum was also used to calibrate the FSR, by comparing a wide (approximately 10 cm^{-1}) FSR-spaced spectrum with the Hitran database (Rothman et al., 2013).

To determine molecular oxygen concentration, the analyzer measures absorption of the Q13Q13 component of the $a^1\Delta_g \leftarrow X^3\Sigma^-_g$ band, at ~~a frequency of~~ 7878.805547 cm^{-1}, according to the latest edition of Hitran (Gordon et al., 2017). This is one of the strongest near-infrared lines of oxygen, well separated from other oxygen lines, and reasonably free of spectral interference from water, carbon dioxide, methane, and other constituents of clean air. The spectral model for this line was developed using reference spectra of clean, dry, synthetic air that were acquired with the same hardware as in the field-deployable analyzer, but with special-purpose software that allows it to operate as a more general spectrometer.

Recently, considerable work has been done to advance the understanding of spectral line shapes and to define functional representations that better describe the processes that

Formatted: English (United States)

determine spectral line shapes than does the Voigt model (Hartmann et al., 2008; Tennyson et al., 2014, Tran et al., 2019). Line shape studies have been published for the 1.27 μm band of O_2 (Fleisher et al., 2015; Lamouroux et al., 2014), though not to our knowledge for the Q branch. The apparatus used here is not capable of spectroscopic studies of comparable precision; the absolute temperature and pressure monitoring and especially the frequency metrology are far too crude for that purpose. Our goal is merely to define a simple model of the Q13Q13 line that is adequate for least-squares retrievals of the O_2 absorption under the limited range of conditions (stabilized temperature and pressure) that the operational analyzer experiences in the field. The CRDS analyzers use the Galatry function (Varghese and Hanson, 1984), which is distinctly better than the Voigt and still easily and quickly evaluated for line shape modeling. Ultimately, the usefulness of the spectral model is to be evaluated by the precision and stability of the O_2 measurements when compared with established techniques. ~~We also note at this point that Sironneau, Fleisher, and Hodges have made detailed measurements of lines in the R branch of the $a^1\Delta_g \leftarrow X^3\Sigma^-_g$ band and observed departures from simple, linear absorption, which they interpret as arising from collision-induced absorption (Fleisher et al., 2015). This has two important consequences for O_2 monitoring: the line strength is not independent of sample pressure, and optical absorption is not linear in laser intensity. We do not expect these effects to be too severe for our application because the ring-down cavity is stabilized to a very narrow range of temperature and pressure. In addition, the optical power in the ringdown cavity set by the ring-down detector threshold, which is used to trigger the laser shutoff and subsequent ring-down waveform acquisition. The fact that all ring-downs occur at the same intracavity power should minimize the effect of collision-induced absorption. We have observed some excess noise on the ring-down time constants for the highest loss points at the peak of the Q13Q13 line, which might have to do with the fitting~~

~~of the ring-down signal if absorption is not linear, but we cannot be certain of this explanation at present.~~ Ultimately, the usefulness of the spectral model is to be evaluated by the precision and stability of the O_2 measurements when compared with established techniques.

Formatted: English (United States)

For spectral model development, this spectrometer has the drawback that the cavity FSR~~, equal to about 0.0206 cm^{-1}~~, is too large to reveal much detail of the absorption line shape, even with the simplifying assumption of a Galatry line shape. We therefore acquired a set of four interleaved spectra, with the PZT-actuated mirror moved to offset the cavity modes of the individual FSR-spaced spectra by one-fourth of an FSR. The precise offsets were determined from fits to the strong and well-isolated O_2 lines in the spectra. From the consistency of the fitted line centers, we estimate that the positioning of the interleaved spectra was accurate to approximately 10 MHz. The spectrum of the Q13Q13 line acquired in this manner is shown in Figure 1, together with the best-fit Galatry function. It stands out that the residuals ~~that~~ are largely ~~an odd function of~~odd in detuning from the line center: this shows the limitations of the Galatry model in this case, since the Galatry function is purely even about the line center. The shape of the absorption line in this model is specified by two dimensionless parameters: the collisional broadening parameter

$$y = \gamma / \sigma_D \qquad (1\text{~~1~~}2)$$

and the collisional narrowing parameter

$$z = \beta / \sigma_D \qquad (2\text{~~2~~}3)$$

where γ is the frequency of broadening transitions, β is the ~~frequency of narrowing collisions~~velocity change collision rate, and σ_D is the 1/e Doppler half-width~~Doppler width~~ of the transition, given by

$$\sigma_D = \nu_0(2k_BT/Mc^2)^{1/2} \qquad (3\text{~~3~~}4)$$

where ν_0 is the transition frequency, k_B is Boltzmann's constant (J. K^{-1}), T is the sample temperature (K), M is the molecular mass (amu), and c is the speed of light (m/s). Figure 2 shows the values of y and z obtained from spectra acquired in the same way as Figure 1, as a function of cavity pressure. The values depend linearly on pressure, as expected from the Galatry model, but the unconstrained linear fits do not go precisely through the origin. It is not clear whether this represents a breakdown of the Galatry model or simply reflects the limited quality of the data set. The slope of y can be converted to an air-broadened collisional width γ_{air} = 0.0442 cm^{-1}/atm, which agrees with the Hitran value of 0.0460 cm^{-1}/atm (~~Rothman et al., 2013~~) (Gordon et al., 2016) to within the uncertainty estimate stated by Hitran (uncertainty code 4 for γ_{air} corresponding to 10% --20% relative uncertainty). The slope of z can be interpreted in terms of the optical diffusion coefficient (Fleisher et al., 2015), yielding D = 0.285 cm^2 s^{-1}, compared to the literature value of 0.233 cm^2 s^{-1} for O_2 in air at 45 °C (Marrero and Mason, 1972). Although the anticipated use of the analyzer is for ambient air samples having a very small range of O_2 concentrations, we did investigate the variation of the line shape in binary mixtures of O_2 and N_2 shown in Figure 3. The error bars are taken from the output of the Levenberg-Marquardt fitting routine (Press et al., 1992). The dependence of the collisional broadening parameter z on O_2 mole fraction was considered too small to be significant, but the variation in y was used in the subsequent analysis of the air samples. Note that Wójtewicz et al. (Wójtewicz et al., 2014) also found collisional broadening coefficients for nitrogen to be slightly larger than for oxygen in measurements of one O_2 line in the B-band.

The primary goal in designing the analyzer was to achieve high enough precision to make meaningful measurements of O_2 in clean atmospheric samples. Although the current best practice for such high-precision measurements is to work with dried samples, we decided

Formatted: Superscript

Field Code Changed

Formatted: English (United States)

Formatted: English (United States)

to include high precision measurements of water vapor. There were two reasons for this decision: one is to serve as a monitor for residual water vapor, which is difficult to remove completely from the ring-down cavity and associated sample handling hardware, and the second and more ambitious reason was to see how well the effect of water vapor could be corrected for ~~in~~ measurements of undried ambient air. While it was considered unlikely that measurements of undried air could compete in accuracy with those of dried air, it might be possible to correct for water vapor well enough to enable useful measurements in some circumstances without the expense and inconvenience of drying the sample. For this purpose, a second laser was added, which probes the $7_{1,6} \rightarrow 8_{4,5}$ component of the $2\nu_3$ band of water vapor, at ~~a frequency~~ of 7816.75210 cm^{-1} (Gordon et al., 2017). The Galatry model was used to fit spectra of synthetic air humidified to various levels of water vapor concentration. These fits also included two other nearby, very weak water lines, with intensities less than 1% of the strong transition, in order that their absorption should not perturb the line shape of the main transition. Results for the shape of the 7816.75210 cm^{-1} line are shown in Figure 4. At the level that we can measure, only the y-parameter has a meaningful variation with water concentration. From the linear fit one obtains a pressure broadening coefficient for air, γ_{air} = 0.0752 cm^{-1}/atm, in reasonable agreement with the Hitran value γ_{air} = 0.0787 cm^{-1}/atm (Gordon et al., 2017), and a self-broadening coefficient γ_{self} = 0.413 cm^{-1}/atm, to be compared with the Hitran value γ_{self} = 0.366 cm^{-1}/atm. Since the uncertainty estimate for the Hitran values is 10 % to 20 %, this level of agreement seems reasonable.

We also looked at absorption from water near the Q13Q13 absorption line of O_2. These spectra were measured in a background of pure nitrogen to reveal the very weak lines interfering with the O_2 measurement. Without the strong O_2 lines, it was impossible to interleave FSR-spaced spectra, so in this case the frequency axis comes from the analyzer's

wavelength monitor. The upper panel of Figure 5 shows the spectrum of saturated water vapor in nitrogen, together with a fit to a Voigt model of the molecular lines. The measurement was made at a pressure of 340 hPa and temperature of 45° C. ~~The two most prominent features in this spectrum are actually the Q17R16 and Q13Q13 lines from traces of O_2 remaining in the sample while the other features are from water.~~ The main features are the Q13Q13 line from trace contamination of oxygen in the sample and several lines that arise from normal water ($^1H_2{}^{16}O$, AFGL code 161) and deuterated water ($^1H^2H^{16}O$, AFGL code 162, also abbreviated HDO). The lower panel of Figure 5 shows the lines tabulated in Hitran. Immediately after the data in Figure 5 were acquired, measurements were also made at 7816.85210 cm^{-1}, to establish the relationship between the absorption strengths in the two spectral regions. ~~All the water lines that were observed, in both spectral regions, are from the dominant 161 isotopolgue of water, so changes in isotopic composition of atmospheric water does not lead to variation in the relative strengths of the lines we measure.~~ The relative intensities of the 161 and 162 lines change with variations in the isotopic composition of the water, but fortunately the direct interference with the oxygen Q13Q13 lines comes entirely from the 161 isotopologue, with the strongest 162 line being separated by approximately 8 line widths (FWHM) from the Q13Q13 line. Hitran simulations for molecules other than water that are expected to be present in clean, ambient air indicate that direct interference with the Q13Q13 line should be negligible at the level of precision considered here. In the case of CO_2, the dilution of oxygen due to 400 ppm of CO_2 is significant, and larger than any direct spectral interference.

Finally, we investigated the influence of water vapor on the shape of the O_2 Q13Q13 line. Switching between the two lasers sources, we acquired FSR-spaced spectra of humidified synthetic air, alternately covering the 7817 cm^{-1} and 7878 cm^{-1} regions. Individual spectra were acquired in less than 2 s, so changes in water vapor concentration between

Formatted: English (United States)

Formatted: English (United States)

Formatted: English (United States)

Formatted: English (United States)

Formatted: Font: Times New Roman, 12 pt, English (United States)

spectra were small. These spectra, with frequency resolution of 0.0206 cm^{-1}, were analyzed by nonlinear least-squares fitting with the following spectral models: the 7817 cm^{-1} spectra were modeled as the sum of an empty-cavity baseline having an adjustable offset level and slope and the water spectrum is modeled with three peaks: one strong line and two weak perturbers~~three water peaks and the two weak perturbing peaks~~. The molecular absorption of the main peak was expressed as an adjustable amplitude, A_w, multiplying a dimensionless, area-normalized Galatry function (Varghese and Hanson, 1984). The weak perturbers were modeled by Voigt profiles with amplitudes and line widths that were constrained to be in fixed ~~ratios~~ proportions to the strong line, and therefore added no new degrees of freedom to the fitting procedure. Since the amplitude A_w multiplies an area-normalized shape function, it is essentially equivalent to the area of the absorption line, to the extent that the Galatry model provides a valid description of the line shape. The Doppler width of the Galatry function was fixed based on the measured cell temperature, the y-parameter was allowed to vary, and the z-parameter was constrained to be proportional to y, based on measurements summarized in Figure 2~~the earlier measurements~~. In addition, the center frequency of the Galatry function was adjusted to match the data set, giving a total of five free parameters for this fit. The 7878 cm^{-1} spectra were modeled with an adjustable baseline offset and slope and molecular absorption amplitude, A_{O2}, describing the Q13Q13 O_2 line. Here, too, the y-parameter and centration of the O_2 lines were allowed to adjust, and the z-parameter was constrained to be proportional to y. The weak water lines interfering with oxygen absorption were included in the model, but with no additional free parameters~~;~~ rather the amplitudes were preset based on the measured water absorption at 7817 cm-1 and the previously determined amplitude relationships between the water lines. This procedure does not account for variations in HDO abundance, which may introduce some systematic error into the water vapor correction for

Formatted: Font: Times New Roman, 12 pt, English (United States)

Formatted: English (United States)

Formatted: Not Superscript/ Subscript

Formatted: Font: Times New Roman, 12 pt, English (United States)

samples of unusual isotopic composition, but it should accurately model the most important lines that interfere with the oxygen measurement. Collisional broadening of the Q13Q13 O_2 line by water vapor is shown in Figure 6. From the linear fit one obtains a coefficient for collisional broadening of the Q13Q13 line by water vapor of γ_{water} = 0.0442 cm^{-1}/atm. We are not aware of previous measurements of this quantity.

The alternating measurements at 7817 cm^{-1} and 7878 cm^{-1} also calibrated the relationship between water mole fraction and the absorption at 7817 cm^{-1}, using a dilution analysis described by Filges et al. (2018) ~~(Filges et al., 2018)~~, who showed that the results obtained this way agree well with water vapor fractions measured with a conventional hygrometer. Figure 7 shows the measured amplitudes of the water and oxygen lines for samples of variable humidity. Since the air came from a tank of constant composition, the oxygen concentration changes due to dilution of oxygen when water is added. Assuming that this is the sole cause of the change in measured absorption, since the line shapes were being constantly adjusted to account for changes in collisional broadening, it is straightforward to deduce the relation between the water fraction and the absorption amplitude. This calibration was used to generate the water fraction axes in Figures 4 and 6. We note that we did not take particular care to control or measure the quantity of dissolved gases, especially oxygen and carbon dioxide, in the water used for this experiment. While these gases would not significantly affect the water calibration, they may affect the water vapor correction of the oxygen measurement at the ppm level. More work needs to be done to investigate the water vapor correction of the oxygen measurement.

The observations described above were used to design a method to measure oxygen concentration in ambient air. Gas from the inlet to the analyzer is drawn through the cavity at a rate of about 100 sccm (standard cubic centimeter per minute) and the conditions in the

Formatted: Font: Times New Roman, 12 pt

cavity are held stable at 340 hPa and 45° C. In its analysis mode the analyzer alternately measures ring-downs in the 7817 cm^{-1} and 7878 cm^{-1} regions. At 7878 cm^{-1} measurements are made at 11 different frequencies, spaced by one FSR of the cavity and centered at the peak of the Q13Q13 line. Multiple ring-down measurements are made to improve the precision of the loss determination, with a total of 305 ring-downs allocated to one spectrum. In the 7817 cm^{-1} region measurements are also made at 11 distinct frequencies at FSR spacings. Only 35 ring-downs are allocated to this spectral region, since the measurement of O_2 is much more important than water vapor. The data sets are analysed using a Levenberg-Marquardt fitting routine, which adjusts five free parameters in each region to find the best agreement to a spectral model based on Galatry line shapes, as described above. One of the outputs of the 7878 cm^{-1} fit is the frequency offset of the FSR grid from the center of the Q13Q13 line. This information is used to adjust the position of the PZT actuated mirror to keep the measurements centered on the line, effectively stabilizing the optical path length of the cavity to the frequency of the O_2 line. The reported water fraction is obtained by multiplying the fitted amplitude of the water line by a calibration constant derived from the dilution experiment as explained above. For the O_2 fraction a slightly more complicated procedure is followed. It was observed that the least-squares fitting of the data gives highly correlated results for the amplitude of the absorption line and the line width parameter y. The correlation may be due in part to the fitting procedure itself (Press et al., 1992) and it may also have a contribution from pressure variations that the pressure sensor is unable to detect. The ratio A_{O2}/y can be determined from the fit much more precisely than A_{O2} alone and so gives a more sensitive measurement of molecular absorption. It also has the advantage of being independent of sample pressure, to the extent that the Galatry model applies (Figure 2). However, using the ratio A_{O2}/y as a metric for absorption adds ~~additional~~ more complications

333 if measurements are to be made over a range of O_2 and water concentrations, because the O_2/
334 N_2 ratio and water concentration affect the line width independently of pressure and O_2
335 concentration alone. To minimize systematic errors due to these broadening effects, we define
336 a nominal y-parameter based on the measured amplitudes of the O_2 and water lines and the
337 line broadening dependences shown in Figures 3 and 4. The measured ratio A_{O2}/y is
338 normalized by the nominal y to obtain a quantity that is ideally independent of pressure and
339 water concentration, and this is the quantity that is multiplied by a calibration constant to give
340 the reported O_2 fraction. In addition, a dry mole fraction is reported for O_2, defined as the
341 directly measured mole fraction corrected for water dilution.

342 The main goal in developing this instrument was to make high precision
343 measurements of O_2 mole fraction, based on absorption by the dominant $^{16}O_2$ isotopologue.
344 The absorption lines of the rarer isotopologues are also present nearby, so a mode of operation
345 was included in which one laser is scanned over neighboring lines of $^{16}O_2$ and $^{16}O^{18}O$ and the
346 ratio of amplitudes is used to derive an isotopic ratio, reported in the usual delta notation. In
347 this case the operating pressure was reduced to 160 hPa to improve the resolution of the
348 nearby lines. The lines measured were the Q3Q3 line of $^{16}O_2$, at 7882.18670 cm^{-1}, and the
349 Q9Q9 line of $^{16}O^{18}O$, at 7882.050155 cm^{-1}. The measurement procedure is very much like
350 that for the O_2 fraction measurement, so it will not be described in detail, only the main
351 differences will be noted. One is that in determining an isotopic ratio, ~~there is no advantage to~~
352 ~~be obtained from~~ normalizing absorption amplitudes to line widths does not provide any
353 advantage, instead we simply take the ratio of amplitudes to compute delta. Although the
354 Q9Q9 line and its neighbor Q8Q8 are the strongest ones in this band, absorption by $^{16}O^{18}O$ is
355 still very weak, only about $5x10^{-9}$ cm^{-1} at the line center under the conditions we used.
356 Consequently, the signal-to-noise that can be achieved with this analyzer is not adequate to

determine both the amplitude and the width of the $^{16}O^{18}O$ line with useful precision, so in the fitting step the y-parameter of the $^{16}O^{18}O$ line is constrained to be a constant factor times the fitted y-parameter for the $^{16}O_2$ line. Additionally, because of the weakness of the rare isotopologue absorption, the majority of ring-downs in each spectrum is devoted to measuring $^{16}O^{18}O$ i.e. 232 ring-downs in each spectrum versus only 40 for $^{16}O_2$. This implies that the mole fraction measurement in the isotopic mode is much less precise than when the analyzer measures the Q13Q13 line alone.

3. Results and Discussions

3.1. Laboratory tests at Picarro, Santa Clara

3.1.1. Temperature and pressure sensitivity

One set of tests was done to determine how well the goal was met of minimizing the susceptibility of the concentration measurements to ~~uncontrolled~~ noise or drift of the sample temperature and pressure. For these tests the analyzer sampled dry synthetic air from a tank and the temperature and pressure setpoints of the cavity were adjusted upward and downward from the nominal values, to obtain an estimate of the differential response. We express the sensitivity to experimental conditions in relative form, that is the derivative with respect to temperature or pressure divided by the signal under nominal conditions.

From these experiments, we determined a temperature sensitivity of -2.1×10^{-4} K^{-1} and a pressure sensitivity of $+9.8 \times 10^{-6}$ hPa^{-1}. The temperature sensitivity is somewhat larger than expected based on a calculation using Hitran data to estimate the temperature dependences of all the quantities that go into the measured absorption of the Q13Q13 line. The pressure sensitivity is strikingly small, indicating a good cancelation of the pressure dependence of absorption amplitude and line width. Both temperature and pressure sensitivities are small enough to have a negligible effect on short-term precision of measurements made with the

stabilized ring-down cavity, though long-term drifts in the sensors are always a matter of concern.

3.1.2. Measurement precision and dDrift

Measurement precision was evaluated by analyzing synthetic air containing nominal atmospheric concentrations of CO_2 and CH_4 from an aluminum Luxfer cylinder over a period of several days. The tank, oriented horizontally and thermally insolated insulated (though not controlled), was connected directly to the instrument (S/N TADS2001) with a 2-stage pressure regulator and stainless-steel tubing and reducing the flow with an additional orifice to about 55 sccm. For the isotopic mode of operation, the precision of the measurement was also tested by making repeated measurements from a tank of clean, dry synthetic air.

Figure 8 shows the time series of the precision test data, displaying the reported oxygen concentration, the height of the oxygen absorption peak, the width of the oxygen absorption peak and the ambient temperature. The residual errordrift of the analyzer, although small, is nevertheless significant given the stringent targets set forth by the WMO-GAW program. Possible sources of drift error include: temperature drifts due to sensor drift or gradients; pressure errors due to sensor drift; optical artifacts such as parasitic reflections, higher order cavity mode excitation, and/or loss nonlinearity that can distort the reported oxygen spectrum. More work is required to identify and eliminate these small drifts.

The Allan standard deviation of the reported O_2 fraction is shown in the Allan-Werle plot in Figure 9. The ordinate on this plot is the square root of the Allan variance of reported mole fraction, so 1 ppm in these units corresponds to about 5 per meg in the ratio of O_2/ N_2. The precision of averaged measurements improves as $\tau^{-1/2}$ for approximately 5000 s and reaches 1 ppm in less than 10 minutes and remains below 1 ppm for time scales on the order of about 1 hour (Tau is the abscissa of the Allan-Werle plot).

Figure 10 shows the precision of $\delta(^{18}O)$ (uncalibrated) derived from the ratio of lines measured at 7882 cm^{-1}. Because of the weak signal from the $^{16}O^{18}O$ line, it is necessary to average for more than 20 seconds or more to achieve 1‰ precision on the isotopic ratio. As for the concentration measurement, averaging improves the measurement precision for times scales up to about 1 hour.

3.2. Laboratory measurements at the University of Bern

3.2.1. Measurements of standard gases

The performance of the instrument was tested by analyzing eight standard gases with precisely known CO_2 and O_2 compositions (Table 1) using the CRDS analyzer and comparing it to parallel measurements with a paramagnetic oxygen sensor (PM1155 oxygen transducer, Servomex Ltd, UK) embedded to a commercially available Oxzilla fuel cell oxygen analyzer (OXZILLA II, Sable Systems International, USA) (Sturm et al., 2006) as well as with an isotope ratio mass spectrometer (IRMS, Finnigan $Delta^{Plus}XP$). The design of the measurement set-up is shown in Figure 11. Standard gases were directly connected to the pressure controlling unit, and a multi-port valve (V2) was used to select among the standard gases. FThe flow from each cylinder was adjusted to about 120 ml min^{-1} sccm which was eventually directed to a selection valve (V1), allowing switching between ambient air and standard gases. Flow towards and out of the Oxzilla fuel cell analyzer was controlled by the pressure controlling unit. The O_2 mixing ratio of this incoming gas was first measured on the Paramagnetic O_2 sensor and then directed towards a non-dispersive infrared analyzer (NDIR) (Li-7000, LICOR, USA) for measuring CO_2 and H_2O. The outflow from this analyzer (100 ml min^{-1} sccm) returns to the pressure controlling unit and was eventually divided between the CRDS analyzer (which uses about 75-80 ml min^{-1} sccm) and the IRMS (~ 20 ml min^{-1} sccm)

via a Tee-junction. Each cylinder was measured for two hours in each system controlled by a LabView ~~VIEW~~ program.

~~In priori~~First, we investigated the influence of this Tee-junction, which splits the gas flow between the CRDS and the IRMS, on the measured O_2 values. Manning (2001) showed that the fractionation of O_2 in the presence of a Tee-Junction is strongly dependent on the splitting ratios as well as temperature and pressure gradients. Hence, we measured and compared the O_2 mixing ratios of two standard gases (CA07045 and CA060943) in two cases: i) in the presence of a Tee-junction with different CRDS to IRMS splitting ratios and ii) without a Tee-junction so that all gas flow is directed towards the CRDS analyzer. The splitting ratios in these test experiments vary from 1:1 to 1:100, and reversed to change the major flow direction either to the CRDS or the IRMS. Note that the experimental condition in this manuscript is with a 4:1 splitting ratio (i.e. ~ 80 ~~ml min^{-1}~~sccm towards the CRDS analyzer and ~ 20 ~~ml min^{-1}~~sccm towards the IRMS).

In the cases of the smaller splitting ratios (1:1, 1:4 and 4:1), which are relevant for the results presented in this study, only minor differences in the measured O_2 mixing ratios were observed when compared to case ~~b~~ ii (i.e. without a Tee-junction). For these two cylinders measured, the average differences in these cases were about 0.5 ppm, calculated as the mean of the differences in the raw O_2 measurements of the last 60 seconds. The negligible fractionation can indeed be the result of smaller splitting ratios while strong influence is usually expected in case of larger splitting ratios (Stephens et al., 2007). For higher splitting ratios, the result seems inconclusive without any dependence on the ratios due to the strong decline in the cylinder temperature (specifically at the pressure gauge) caused by higher flow to achieve the higher splitting ratios (as high as 1:100). Hence, these tests need to be

conducted in a temperature controlled condition and the results could not be discussed in this manuscript.

Figure 12 shows the standard gas measurements for the seven cylinders with known CO_2 and O_2 mixing ratios (Table 1) using both the CRDS and the Paramagnetic analyzers. Standard eight, which has too high O_2, is not shown in the figure as the figure is zoomed-in to better illustrate the change in O_2 for the remaining cylinders. While the first five cylinders contain O_2 and CO_2 mole fractions comparable to ambient air values, standards 6 & 8 had either very low ~~and~~ or very high O_2, respectively. In addition, standards 6 and 7 have very low and very high CO_2 mixing ratios. Note that due to its very high CO_2 content (~ 2700 ppm), standard 7 was not measured on the IRMS and hence the O_2 mixing ratio~~s~~ ~~are~~ is unknown. The measured mixing ratios for the six standard gases ~~between~~ measured with the two systems are in very good agreement while cylinder 7 showed an opposing signal for the two analyzers compared to standard 6 (Figure 12). While the Paramagnetic analyzer showed a higher O_2 mixing ratio, the values from the CRDS analyzer are lower in O_2. This can be associated with the very high CO_2 mixing ratio in standard 7, which leads to a strong dilution effect in the CRDS analyzer as it does not include any correction function for dilution effect from CO_2. However, such high CO_2 mixing ratios may not be that important for most atmospheric research. Yet, it should be considered to include a parallel CO_2 mixing ratios measurement to the instrument as it will further improve the accuracy. This would be especially important for biological or physiological studies where a wide range of CO_2 and O_2 concentrations must be expected.

The measurement precision of the CRDS analyzer was calculated as the standard error of the mean i.e. the standard deviation (1-σ) of the last 1-minute raw measurements divided by the square root of the number of measurements (n = 60), and for all these cylinders the

values are usually between 0.5 ppm to 0.7 ppm. For parallel measurements of these cylinders using a Paramagnetic analyzer, we obtained a precision of about 1 ppm, calculated exactly the same way.

We also made a correlation plot to see which of the two instruments are in better agreement with the assigned values based on IRMS measurements for the individual cylinders. While similar correlation coefficients were observed for both analyzers, different slopes were calculated (Fig. A.1). This is due to the fact that the IRMS measures the O_2 to N_2 ratio ($\delta(O_2/N_2)$) in per meg, while the CRDS and the Paramagnetic analyzers provide non-calibrated O_2 mixing ratios in units of ppm and per meg, respectively. If we exclude the two standard gases with the highest and lowest O_2 mixing ratios (standards 7 and 8) that are subjected to strong dilution effects, both the slope and the r^2 values decrease from those shown in Figure A.1. But this decrease is larger in the case of the Paramagnetic measurements, implying a slightly better linearity of the CRDS analyzer.

3.2.2. Measurements of ambient air

Ambient air measurements were conducted from the roof top of our laboratory at the University of Bern to evaluate the analyzer's performance under atmospheric variability. Ambient air was continuously aspirated from the inlet at the roof of the building at a flow rate of ~ 250 ~~ml min^{-1}~~sccm which is then dried using a cooling trap kept at -90 °C towards the switching valve (V1) and measured in similar way to the standard gases as explained above. The measurement values obtained here were compared with the parallel measurements by the Paramagnetic sensor to test the instruments stability and accuracy.

Figures 13 panels a &b show the 1-minute average ambient air measurements from the rooftop inlet by the Paramagnetic and the CRDS analyzers at the beginning of the testing period including standard gases measured every 12-hour. While the Paramagnetic analyzer

seems to be stable, the CRDS analyzer showed a strong drift for an extended period. This can be due to unstable conditions in the CRDS measurement system as it started operating right after it was unpacked. Hence, we looked into temperature inside the instrument chassis~~its DAS temperature~~ and pressure records, which were stable within the manufacturer's recommended range during this period. As the CRDS analyzer incorporates a water correction function, interference from this species should be well accounted. Even comparing the analyzer's parallel water measurements to water measurements by the NDIR system such a drift was not observed. It should be noted that the two internal standard gases which were less frequently measured (every 12 hours) during this period were also drifting ~~in~~ following similar pattern. This implies that the drift is associated with the analyzer. Interestingly, this pattern ~~we observed that the two cylinders follow exactly the same drift pattern that~~ can be modeled using a polynomial function which can then be used to correct for the observed drift in the ambient air measurements. After applying a polynomial drift correction, we were able to fully accounted for the observed drift. However, the manufacturer decided to further investigate possible causes of this drift. After further improvements, we obtained the first commercial analyzer in September 2017 and repeated the above tests (Figure 13 c &d). No such drift was observed any more in the standard gases or in ambient air measurements.

We believe that the optical amplifier has caused the drift in the first system and not anymore included in the design of the product which produced a significant amount of broadband light that could fill the cavity (albeit with a low coupling coefficient), and would ring down with a different (and generally much faster) time constant that the baseline loss of the cavity. However, the ringdown time on the peak of the oxygen line is just 10 microseconds, such that the broadband light might have distorted the single exponential decay of the central laser

Formatted: English (United States)

frequency, leading to the observed drift in the oxygen signal. However, we were not able to confirm this hypothesis.

3.2.3. Water correction test

Measurements of oxygen are reported as both wet ($O_{2,\ raw}$) and dry ($O_{2,\ dry}$) mole fractions by the CRDS analyzer as it also measures water vapor in parallel at its water absorption line (7817 cm^{-1}), and corrects for the dilution effect based on an inbuilt numerical function:

$$O_{2,dry} = \frac{O_{2,raw}}{1 - f_{H_2O}} \qquad (45)$$

where f_{H2O} is the measured water mole fraction.

The efficiency of water correction by this function was assessed in two ways: i) by comparing the water vapor content in standard air measured by this analyzer with similar measurements by the NDIR analyzer and ii) by comparing the oxygen mixing ratios between non-dried ambient air measured and corrected for water dilution by the CRDS analyzer with dried air measured using a paramagnetic analyzer.

Figure 14 shows the water vapor content for standard gases measured continuously for two days by the CRDS and the NDIR analyzers. Note that the two data sets are manually fitted to each other as the measured water values by the NDIR analyzer are not calibrated. Based on ~~these~~ this plot~~s~~, the two analyzers are in very good agreement although there are small differences during very dry conditions (low water content).

Figure 15a shows the dried ambient air water measurements in both analyzers with frequent spikes due to valve switching while measuring standard gases. In the second case, where the water trap was by-passed and non-dried air was allowed to the CRDS analyzer

keeping the dried air flow to the NDIR (Figure 15b), a clear increase in the water measurements in the CRDS analyzer can be observed. Here, it should be noted that there are no spikes in the water measurements of the CRDS analyzers as there are no standard gas measurements in between and the inlet is directly connected to the CRDS analyzer (Figure 11). ~~The water correction test was conducted by measuring dried ambient air (Figure 15a) into both analyzers as well as allowing non-dried air to the CRDS analyzer only (Figure 15b) and comparing the difference in O_2 measurements in both cases (~~Figures 15c & 15d~~).~~ show~~s~~ the difference in oxygen measurements ~~water contents of dried~~ of ambient air measured in both analyzers ~~while Figure 15b shows in case non-dried air is admitted to the picaro analyzer only~~ in the two cases stated above (note that the CRDS uses its ~~in~~ built-in water correction function applying Eq. 5). The measurements of the Paramagnetic analyzer were scaled to ppm units by applying the correlation equation obtained from the six standard gas measurements of the two analyzers (Fig. A.1). Note that the CRDS measurements were corrected for the observed drift using the polynomial fit to the two standard gas measurements stated above.

In the first period of the measurement when both analyzers measured dried ambient air, the absolute differences between the 1-minute averages measured over two days by the two analyzers were mostly within 15 ppm (Figure 15c) and symmetrically distributed around zero (Figure 15e). However, when wet air was admitted to the CRDS analyzer and the in-built water correction was applied, a stronger variability was observed in the calculated differences (Figure 15d). This implies stronger short term variability in the CRDS analyzer measurement values (as nothing was changed for the Paramagnetic measurement system) when wet samples were analyzed. The more negative values in the differences (Figure 15f) can also be associated with overestimation of the O_2 mixing ratios by the CRDS originating from an

568 overestimated water correction. However, detailed evaluation of the analyzer's water
569 correction function is beyond the scope of this study.

570 **3.3. Field Measurements**

571 After a series of tests at University of Bern, we conducted multiple field measurements
572 at the High Altitude Research Station Jungfraujoch and the Beromünster tall tower sites in
573 Switzerland described below.

574 3.3.1. Tests at the High Altitude Research station Jungfraujoch

575 The High Alpine research station Jungfraujoch is located on the northern ridge of the
576 Swiss Alps (46° 33′ N, 7° 59′ E) at an elevation of 3580 m a.s.l. It is one of the global
577 atmospheric watch (GAW) stations well-equipped for measurements of numerous species and
578 aerosols. The site is above the planetary boundary layer most of the time due to its high
579 elevation (Henne et al., 2010; Zellweger et al., 2003). However, thermally uplifted air from
580 the surrounding valleys during hot summer days or polluted air from the heavily industrialized
581 northern Italy may reach at this site (Zellweger et al., 2003). The Division of Climate and
582 Environmental Physics at the University of Bern has been monitoring CO_2 and O_2 mixing
583 ratios at this site based on weekly flask sampling and continuous measurements since 2000
584 and 2004, respectively (Schibig et al., 2015). The CO_2 mixing ratio is measured using a
585 commercial NDIR analyzer (S710 UNOR, SICK MAIHAK) while O_2 is measured using the
586 Paramagnetic sensor (PM1155 oxygen transducer, Servomex Ltd, UK) and fuel cells (Max-
587 250, Maxtec, USA) ~~embedded within~~installed inside a home-built controlling unit. Similar to
588 the comparison tests at the University of Bern, we have conducted parallel measurements
589 between the CRDS analyzer and the paramagnetic cell at this high altitude site during 03 – 14
590 February 2017. The measurement of ambient air at the Jungfraujoch system is composed of
591 sequential switching between ~~a~~ low span (LS) and high span (HS) calibration gases followed

592 by a target gas (T) measurement (once a day) to evaluate the overall system performance and
593 finally a working gas (WG) measurement before switching back to ambient air.
594 Figure 16 (top panel) shows the calibrated 1-minute averaged O_2 mixing ratios
595 measured at this high altitude site in comparison with the Paramagnetic oxygen analyzer
596 already available at the site. ~~While a~~ Despite the strong variability ~~was~~ observed during the
597 measurement period of 10-days by both analyzers, a very good agreement was observed
598 between them.
599 Figure 16 (bottom panel) shows the absolute difference of 1-minute averages in
600 atmospheric O_2 measured at Jungfraujoch between the two analyzers which are mostly within
601 ±5 ppm range (but sometimes going as high as ±10 ppm) without an offset. However, for
602 generally reported 10-minutes, half-hourly or hourly means these values correspond to < 1.5
603 ppm, < 1 ppm and < 0.65 ppm.
604 3.3.2. Tests at the Beromünster tall tower site
605 The Beromünster tower is located near the southern border of the Swiss Plateau, the
606 comparatively flat part of Switzerland between the Alps in the south and the Jura mountains
607 in the northwest (47° 11′ 23″ N, 8° 10’ 32″ E, 797 m a.s.l.), which is characterized by intense
608 agriculture and rather high population density. A detailed description of the tower
609 measurement system as well as a characterization of the site with respect to local
610 meteorological conditions, seasonal and diurnal variations of greenhouse gases, and regional
611 representativeness can be obtained from previous publications (Berhanu et al., 2016; Berhanu
612 et al., 2017; Oney et al., 2015; Satar et al., 2016). The tower is 217.5 m tall with access to five
613 sampling heights (12.5 m, 44.6 m, 71.5 m, 131.6 m, 212.5 m) for measuring CO, CO_2, CH_4
614 and H_2O using Cavity Ring Down Spectroscopy (Picarro Inc., G-2401). By sequentially
615 switching from the highest to the lowest level, mixing ratios of these trace gases were

Formatted: Highlight

616 recorded continuously for three minutes per height, but only the last 60 seconds were retained
617 for data analysis. The calibration procedure for ambient air includes measurements of
618 reference gases with high and low mixing ratios traceable to international standards (WMO-
619 X2007 for CO_2 and WMO-X2004 for CO and CH_4), as well as target gas and more frequent
620 working gas determinations to ensure the quality of the measurement system. From two years
621 of data a long-term reproducibility of 2.79 ppb, 0.05 ppm, and 0.29 ppb for CO, CO_2 and
622 CH_4, respectively was determined for this system (Berhanu et al., 2016).

623 Between 15.02.2017 and 02.03.2017, we have connected the new CRDS oxygen
624 analyzer in series with the CO_2 analyzer (Picarro G-2401) and measured the O_2 mixing ratios
625 at the corresponding heights. Similar to the CO_2 measurements, O_2 was also measured for
626 three minutes at each height. During this period, we have evaluated the two features (isotopic
627 mode and concentration mode) of the CRDS analyzer. In the isotopic mode, the CRDS
628 measures the $\delta^{18}O$ values as well as the O_2 concentration while in concentration mode only
629 the latter was measured.

630 During the tests conducted at this tower site, we first evaluated the two operational
631 modes (concentration vs isotopic modes) of the CRDS analyzer. Ambient air measurements
632 on isotopic mode over a 4-days period showed a strong variability in the measured oxygen
633 mixing ratios and it was not possible to distinguish the variability in the O_2 mixing ratios
634 among the five height levels. The calculated 1-minute standard error for ambient air
635 measurements was as high as 10 ppm while a standard error of less than 1 ppm was
636 determined from similar measurements in the concentration mode. Additionally, comparing
637 the O_2 values between the two modes, frequent short time variation in ambient air O_2 (~ 200
638 ppm) was observed in the isotope mode measurements while the variation in the concentration
639 mode is significantly smaller (~ 30 ppm). This precision degradation is due to the weaker ^{16}O

oxygen line used for the isotopic mode, and the fact that far more ring-downs are collected on the rare isotopologue in isotopic mode Hence, we have conducted the remaining test measurements in concentration mode.

As this tower has five sampling height levels, we first followed three minutes of switching per inlet level, which enables four measurements per hour at a given level. However, we noticed hardly any difference among the different levels due to strong short term variability in O_2 mixing ratios between the consecutive heights. Hence, we switched to a longer sampling period of six-minutes per height. Figure 17 shows the diurnal CO_2 and O_2 variations at the lowest (12 m) and highest (212.5 m) sampling heights of the tower. These two heights were selected simply to better illustrate the difference in the mixing ratios. The CO_2 mixing ratios on the top panel show higher values at the 12 m inlet than the highest level most of the day due to its closeness to sources except during the afternoon (11:00 - 17:00 UTC) when both levels show similar but decreasing CO_2 mixing ratios. This is due to presence of a well-mixed planetary boundary layer (PBL) (Satar et al., 2016). The lag in CO_2 peak between the two height levels by about two hours indicates the duration for uniform vertical mixing along the tower during winter 2017. The opposite variability patterns are also clearly visible in the O_2 mixing ratios shown in the lower panel with a clear distinction between the two height levels during early in the morning and in the evening while similar O_2 values were observed in the afternoon. These opposing profiles are expected as CO_2 and O_2 are linearly coupled with a mean oxidation ratio of -1.1 ± 0.05 (Severinghaus, 1995) for land-biospheric processes (photosynthesis and respiration) and -1.44 ± 0.03 for fossil fuel burning (Keeling, 1988b).

Table 2 shows the oxidation ratios derived as the slopes of the linear regression between CO_2 and O_2 mixing ratios at the different height levels measured on 25 February

2017. Accordingly, height dependent slopes were observed with a slope of -0.98 ± 0.06 at the lowest level, close to the biological processes induced slope but slightly lower than its mean value. For the highest level, we calculated a slope of -1.60 ± 0.07 a value close to fossil fuel combustion oxidation ratio. Note that depending on fossil fuel type the oxidation ratio can range between -1.17 and -1.95 for coal and natural gas, respectively (Keeling, 1988b). While the slopes derived for the two other levels (44.6 m and 131.6 m) show similar values between the highest and lowest height levels, possibly from mixed sources, the middle level showed a slightly higher slope than these two levels but still in the large range between the lowest and highest inlet heights.

3.4. Evaluation of the $\delta^{18}O$ measurements

To further evaluate the analyzer's performance in measuring stable oxygen isotopes, we conducted ambient air isotopic composition measurements as well as analyzed a standard gas without CO_2 which has a known $\delta^{18}O$ value. The choice of this CO_2-free air standard gas is twofold: one it has a known $\delta^{18}O$ value and second as it has no ~~CO_2 possible~~ interference from- possible CO_2 absorption ~~b~~band overlap ~~is avoided~~. For this test three 0.5 L glass flasks were preconditioned and filled with this standard gas to ambient pressure. These flasks were attached before or after the water trap (Fig. 11) and measured similar to ambient air measurements. These measurements were then compared with $\delta(^{34}O/^{32}O)$ values obtained by parallel measurements using our IRMS.

Figure 18 shows the $\delta^{18}O$ values of ambient air from the roof top with three consecutive measurements of glass flasks filled with CO_2-free air in-between followed by a fourth flask filled with breath air. An excellent agreement was observed for measurements from both instruments for the three flasks filled with a standard gas. However, the fourth flask with breath air showed a signal opposite to the measurements by the IRMS. As breath air

contains large amount of water and CO_2 in addition to O_2, which can possibly interfere with the CRDS analyzer measurements, we have removed H_2O and CO_2 by using a cryogenic trap (-130 °C) and in an additional experiment using Schütze reagent to remove both CO and CO_2. However, we have not observed any improvement towards an agreement with the IRMS measurements. Therefore, any other gas component in the breath air must be relevant for the interference. Based on the absorption lines in the spectral range of the instrument (7878 cm^{-1}) retrieved from HITRAN database, we expect interference either from carbon monoxide (now excluded by the tests) or methane or VOCs including acetone, ethanol, methanol or isoprenes, all of which have been measured in breath air (Gao et al., 2017; Gottlieb et al., 2017; Mckay et al., 1985; Ryter and Choi, 2013; Wolf et al., 2017). Further investigations have to shed light on these interferences in order to take corresponding action to surpass these shortcomings in the isotope analysis based on cavity ring-down spectroscopy.

4. Conclusions

We have thoroughly evaluated the performance of a new CRDS analyzer which measures O_2 mixing ratios and isotopic composition combining laboratory and field tests. Even if a drift in the analyzer was observed at the beginning of this study, which ~~if it appears~~ can be easily corrected by calibration, the recent analyzers built by the manufacturer did not show such instrumental drift. However, prior tests are recommended to see the analyzer's stability.

The T-split tests for the current measurement setup based on the measurements of two standard gases showed a difference within the measurement uncertainty. However, this effect may become significant while applying larger splitting ratios and we recommend conducting further experiments to accurately quantify this influence for larger splitting ratios.

We have observed a strong influence of dilution in the measured O_2 values during the presence of high CO_2 mixing ratios. Even if such an influence may not be critical for the present study, such an effect might be significant in other studies where higher CO_2 mixing ratios might be present and we recommend following a correction strategy based on parallel CO_2 measurements. This also applies for more accurate analysis.

The water correction applied by the instrument's in-built function seems to sufficiently correct for the water vapor influence. However, a larger variability of the difference was observed between the CRDS analyzer and the Paramagnetic cell when dried samples were used in both systems. This can possibly be due to an overcorrection by the water correction function of the CRDS analyzer when dried samples were used. This is particularly true for the very low water vapor range (< 100 ppm). We believe that it is important to further investigate this issue and identify an improved water correction strategy.

Based on the analysis of O_2 mixing ratios in the concentration and isotopic modes, we have observed ~~about~~ a significant decrease in precision (about ten-fold) in the latter measurement mode. The measured $\delta^{18}O$ values for the standard air by the CRDS analyzer are in excellent agreement with the IRMS values. However, such measurements for a breath air showed a contrasting signal, possibly due to interference from other gases such as CH_4. ~~as breath air contains CO_2, CH_4 and CO in addition to oxygen.~~ Hence, we recommend further investigation on such possible contaminants and how to possibly remove them while conducting ambient air measurements. However, we believe that this analyzer can be used for tracer experiments where artificially enriched isotopes are used to study biological processes such as photosynthesis in plants using isotopically labelled CO_2 and H_2O.

Formatted: Subscript

Acknowledgement

We would like to thank ICOS-RI and the Swiss National Science Foundation (SNF) for funding ICOS-CH (20FI21_148994, 20FI21_148992). We are also grateful to the International Foundation High Alpine Research Stations Jungfraujoch and Gornergrat. The measurement system at the Beromünster tower was built and maintained by the CarboCount-CH (CRSII2_136273) and IsoCEP (200020_172550) projects both funded by SNF.

List of Tables

Table 1. Assigned mixing ratios of standard gases used in this study and their corresponding values measured by the NDIR, CRDS and IRMS at the University of Bern. [1]The assigned values are based on measurements from different institutions (University of Bern (UB), Scripps or NOAA, see column cylinder name). [2]Measurements are on the Bern scale for CO_2 and O_2. The Bern scale is shifted by +550 per meg. [3]Values on the Scripps scale.

Cylinder name	Assigned CO_2 (ppm) [1]	Assigned O_2 (per meg) [1]	CO_2-IRMS (ppm) [2]	CO_2-NDIR (ppm) [2]	O_2-IRMS (per meg) [2]	O_2-Paramagnetic (per meg) [2]	O_2-CRDS (per meg)[2]
ST-1 LUX3576-UB	427.47	-1026	427.47	427.59	-1026	-1070	-1057
ST-2 LK922131-UB	368.09	599	368.09	367.82	599	560	590
ST-3 CA07045-Scripps	382.303	-271.6	382.50	381.99	278 (-272.2)[3]	302	281
ST-4 CA07043-Scripps	390.528	-476.4	390.69	390.15	71 (-479.5)[3]	66	63
ST-5 CA07047-Scripps	374.480	-807.7	374.70	374.17	-253 (-803.3)[3]	-212	-233
ST-6 CA04556-NOAA	192.44	-3410	191.21	191.64	-3410	-2905	-3013
ST-7 CA06943-NOAA	2699.45	-		2612.80	-	-2691	-3369
ST-8 LK76852-UB	411.49	37794	411.49	406.25	37794	34513	36017

758

759

760 Table 2. The CO_2 and O_2 correlation coefficients at the different height levels derived using
761 the least square fit and the correlation coefficients (r^2). Uncertainties are calculated as
762 standard error of the slope.

Height	Oxidation Ratios (O_2:CO_2)
12.5 m	-0.98 ± 0.06 (0.48)
44.6 m	-1.29 ± 0.07 (0.50)
71.5 m	-1.49 ± 0.08 (0.47)
131.6 m	-1.23 ± 0.05 (0.55)
212.5 m	-1.60 ± 0.07 (0.61)

763
764
765
766
767
768
769
770
771 List of Figures

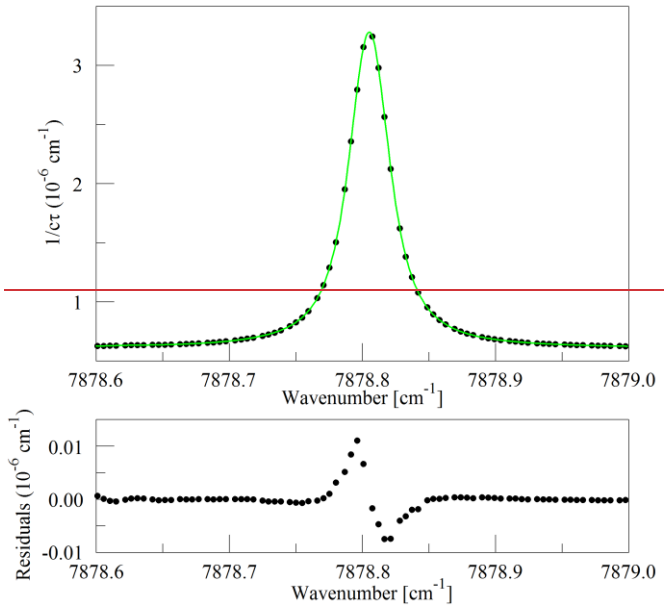
3
2
1
1/cτ (10^-6 cm^-1)
7878.6
7878.7
7878.8
7878.9
7879.0
Wavenumber [cm^-1]
0.01
0.00
-0.01
Residuals (10^-6 cm^-1)
7878.6
7878.7
7878.8
7878.9
7879.0
Wavenumber [cm^-1]

772

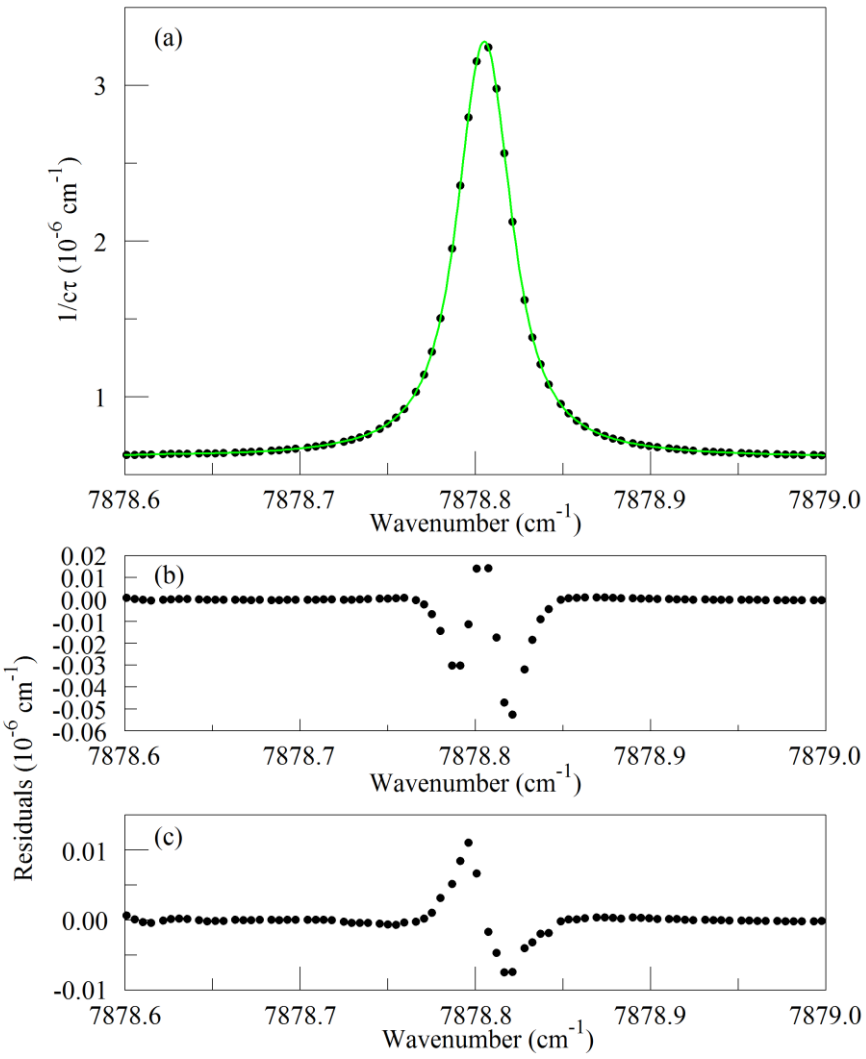

773

774 Figure 1. ~~The Q13Q13 line of O_2 measured in a sample of synthetic air at a sample~~

775 ~~temperature and pressure of 45° C and 333 hPa, respectively.~~

776 The top panel (a) shows the raw data (points) and the best-fit Galatry function (solid line). Residuals

777 of the Voigt fit are shown in panel (b) and residuals of the Galatry fit are shown in panel (c)

Formatted: English (United States)

778

779

780

781

782

783

784

785

786

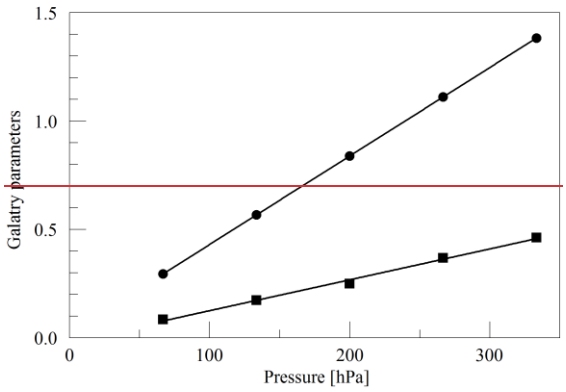

787

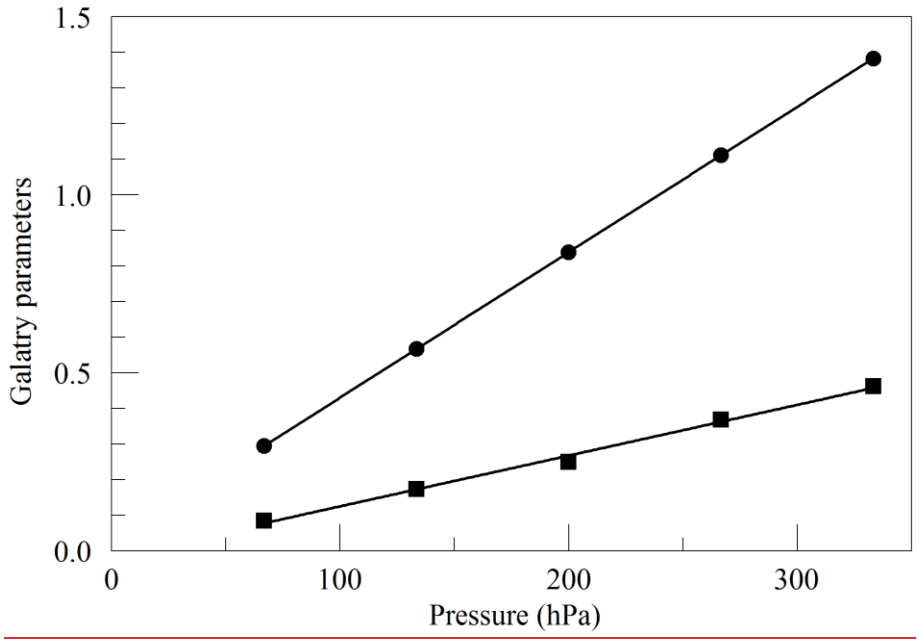

788

789 Figure 2. Best-fit values for the Galatry parameters of the Q13Q13 line of O_2, as a function of
790 pressure. The line broadening parameter y is represented by circles and the line narrowing
791 parameter z by squares. The solid lines are linear fits to the measurements. The best-fit offset
792 and slope are 0.0227 and 0.004082 hPa^{-1} for y, and -0.0169 and 0.001424 hPa^{-1} for z.

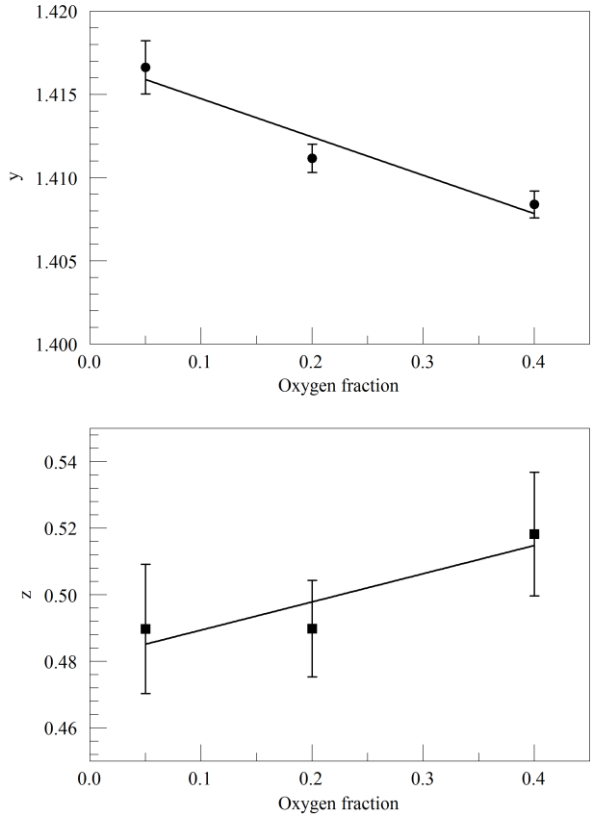

793

794 Figure 3. Galatry parameters of the Q13Q13 line of O_2 at 340 hPa and 45° C as a function of

795 O_2 mole fraction in binary O_2 - N_2 mixtures.

796 The linear fits to the data are $y = 1.417 – 0.023 \times f_{O2}$ and $z = 0.481 + 0.085 \times f_{O2}$.

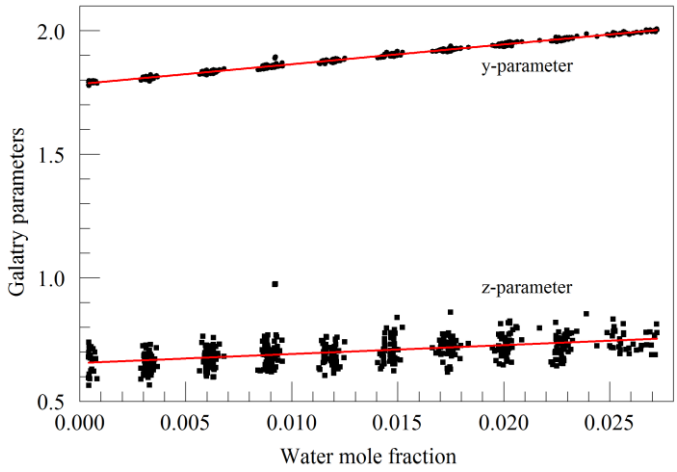

797

798 Figure 4. Galatry parameters of the 7816.75210 cm^{-1} water line in air at 340 hPa and 45° C as

799 a function of water mole fraction. Black points are from measurements and red lines are

800 linear fits: $y = 1.7846 + 8.01 \times f_{H2O}$ and $z = 0.656 + 3.60 \times f_{H2O}$.

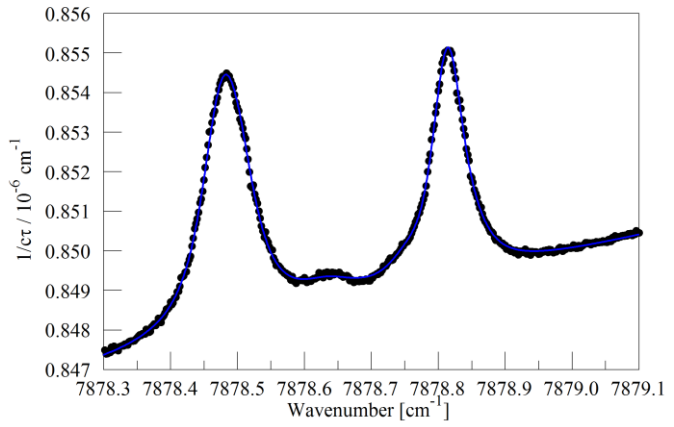
0.856
0.855
0.854
0.853
0.852
0.851
0.850
0.849
0.848
0.847
1/cτ / 10^-6 cm^-1
7878.3 7878.4 7878.5 7878.6 7878.7 7878.8 7878.9 7879.0 7879.1
Wavenumber [cm^-1]

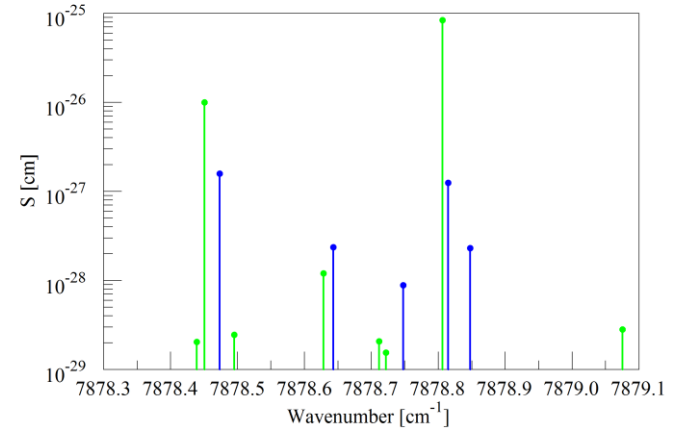
10^-25
10^-26
10^-27
10^-28
10^-29
S [cm]
7878.3 7878.4 7878.5 7878.6 7878.7 7878.8 7878.9 7879.0 7879.1
Wavenumber [cm^-1]

801

802

803

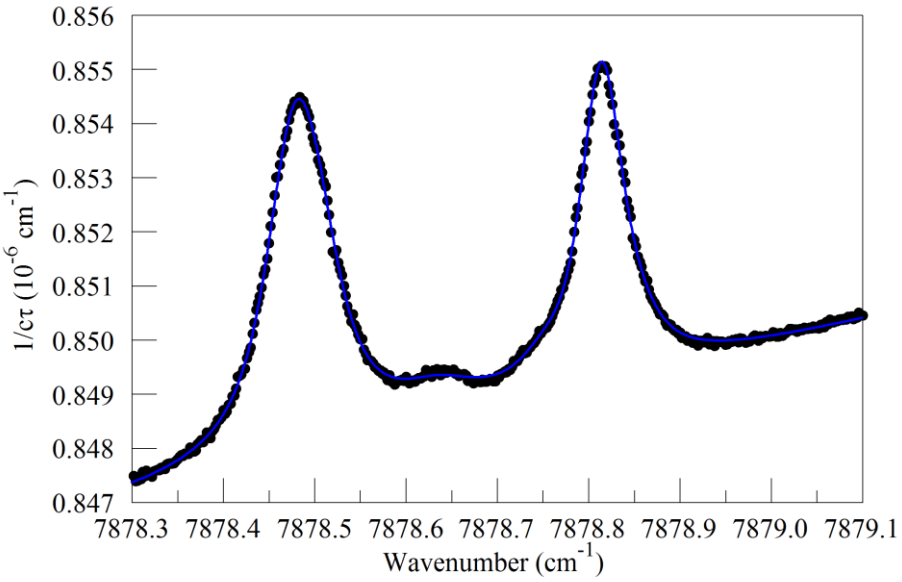
0.856
0.855
0.854
0.853
0.852
0.851
0.850
0.849
0.848
0.847
1/cτ (10^-6 cm^-1)
7878.3 7878.4 7878.5 7878.6 7878.7 7878.8 7878.9 7879.0 7879.1
Wavenumber (cm^-1)

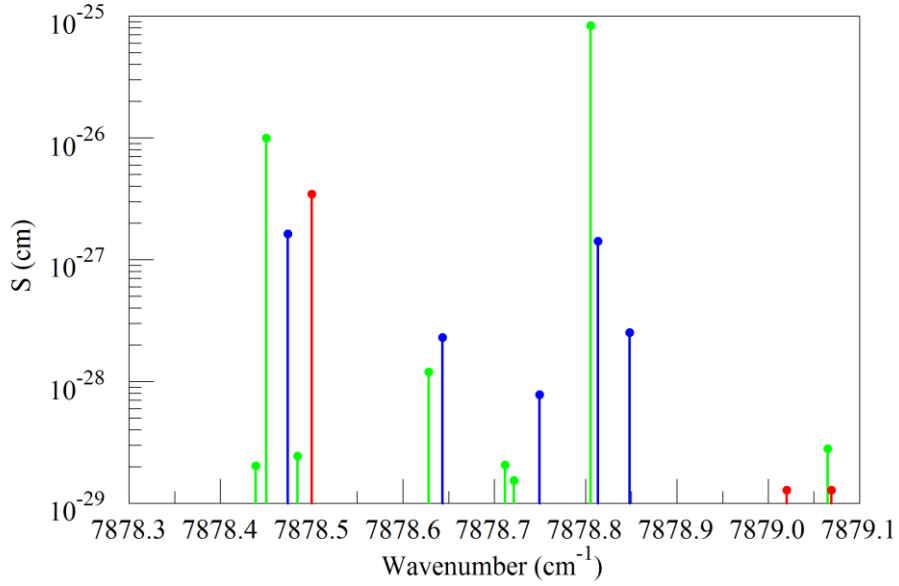
10^-25
10^-26
10^-27
10^-28
10^-29
S (cm)
7878.3 7878.4 7878.5 7878.6 7878.7 7878.8 7878.9 7879.0 7879.1
Wavenumber (cm^-1)

804

Figure 5. Upper panel: spectrum of water in nitrogen (points) and fit to Voigt model (blue curve). Lower panel: Oxygen (green), normal water (blue), and deuterated water (red) lines in the 2016 Hitran data base.~~Figure 5. Upper panel: spectrum of water in nitrogen (points) and fit to Voigt model (blue curve). Lower panel: Oxygen (green) and water (blue) lines in the Hitran database.~~

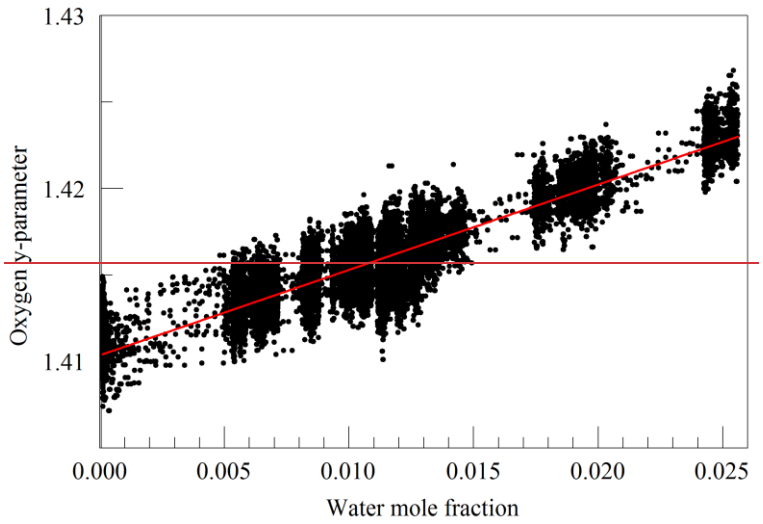

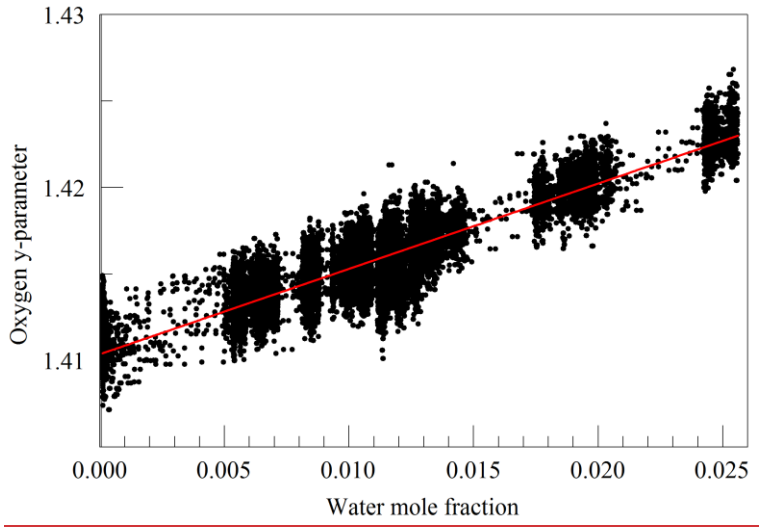

Figure 6. Galatry collisional broadening parameter of the oxygen Q13Q13 line at 340 hPa and 45° C versus water mole fraction. Black points are from measurements and the red line is a linear fit: $y = 1.4109 + 0.467\ f_{H2O}$.

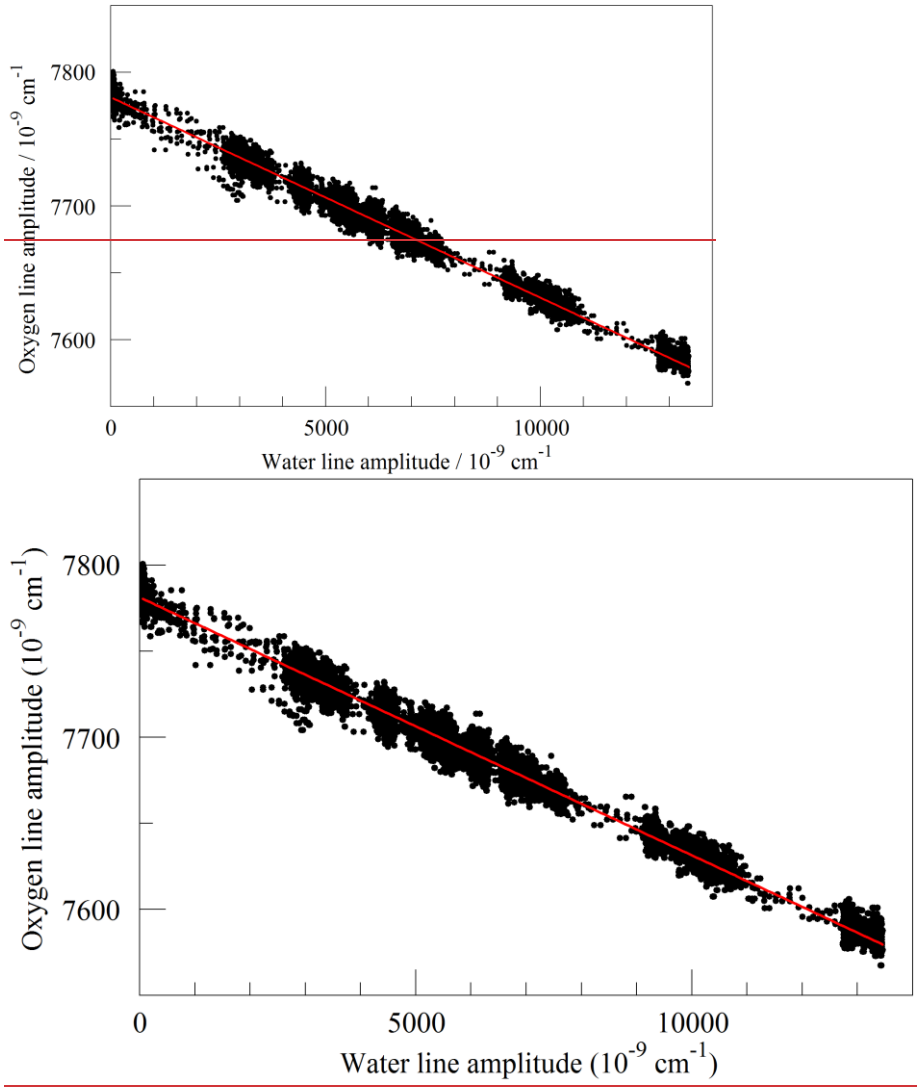

Figure 7. Measured absorption line amplitudes for oxygen and water vapor for water vapor mixing ratios ranging from nearly 0 to 0.025. Black points are from measurements and the red line is a linear fit: with intercept 7.78001 x 10^{-6} cm^{-1} and slope -0.014807.

Formatted: German (Germany)

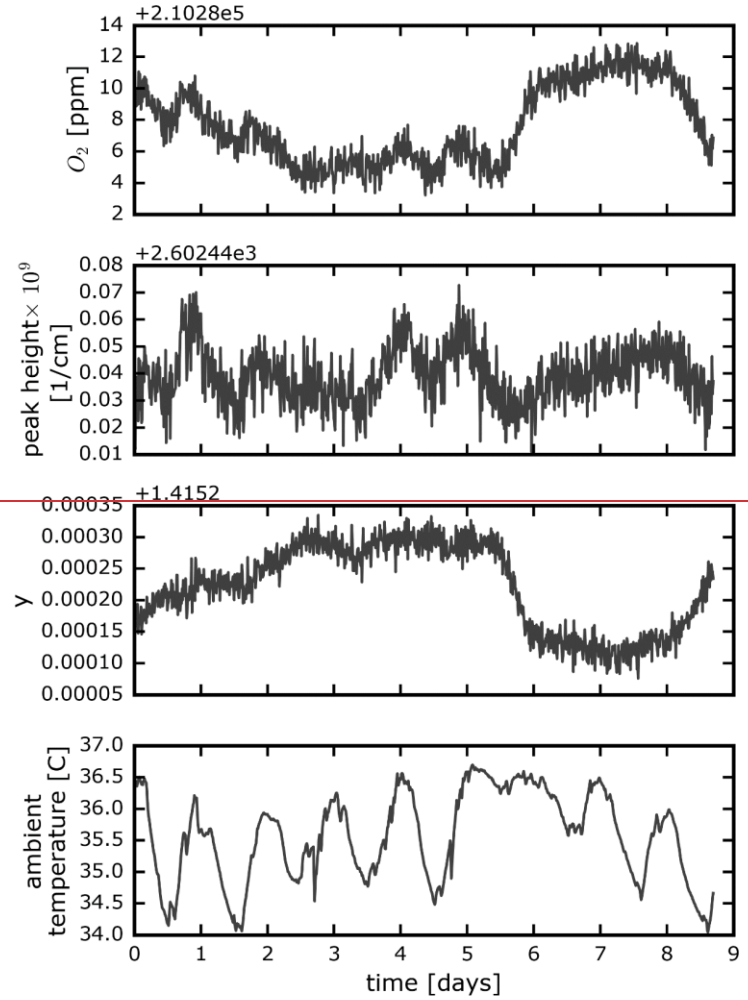
+2.1028e5
O_2 [ppm]
+2.60244e3
peak height$\times 10^9$ [1/cm]
+1.4152
y
ambient temperature [C]
time [days]

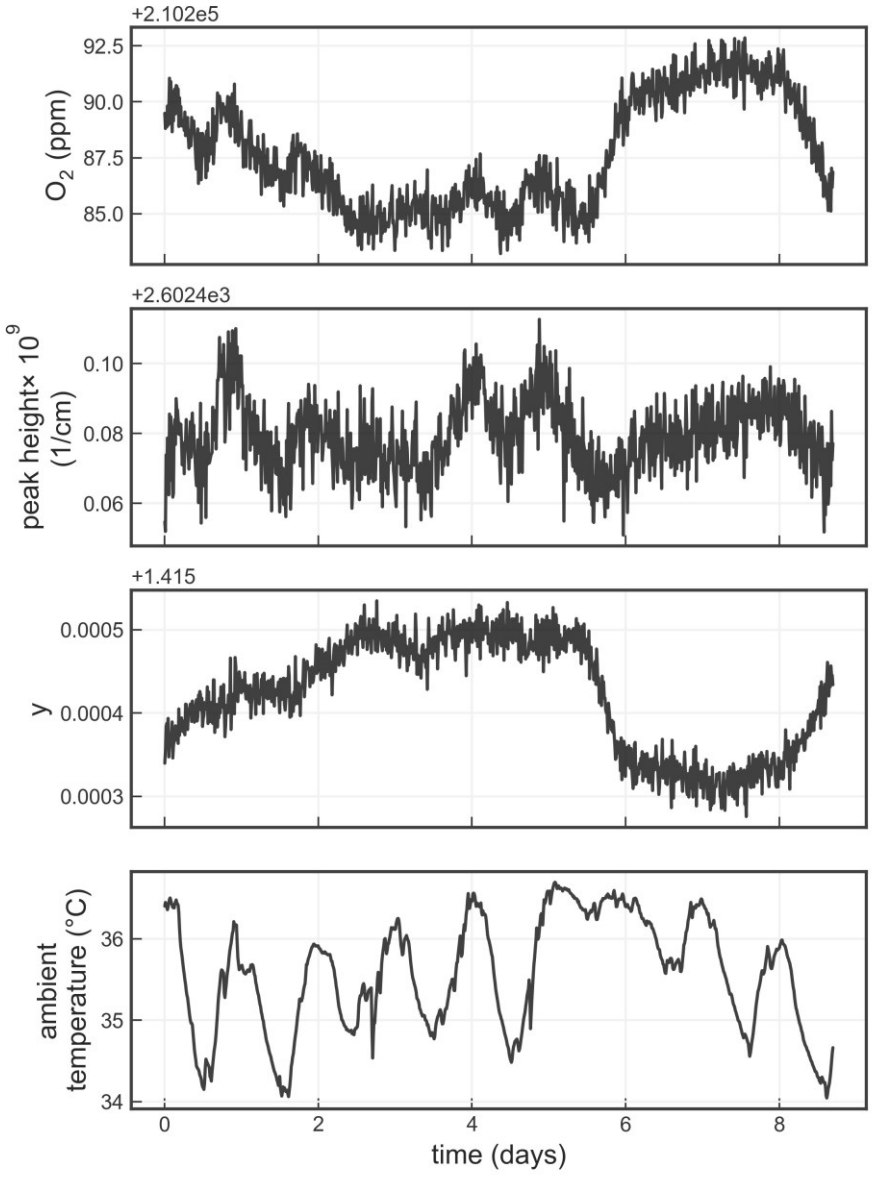

Figure 8. Time series from a measurement of a single tank over about a week. The four panels show~~n~~ the water-corrected oxygen concentration, the absorption peak loss minus the baseline

834 loss, the measured Lorentzian broadening factor, and the ambient temperature (measured in
835 the instrument housing), respectively. A windowed average of 300 seconds was applied to all
836 four data sets.

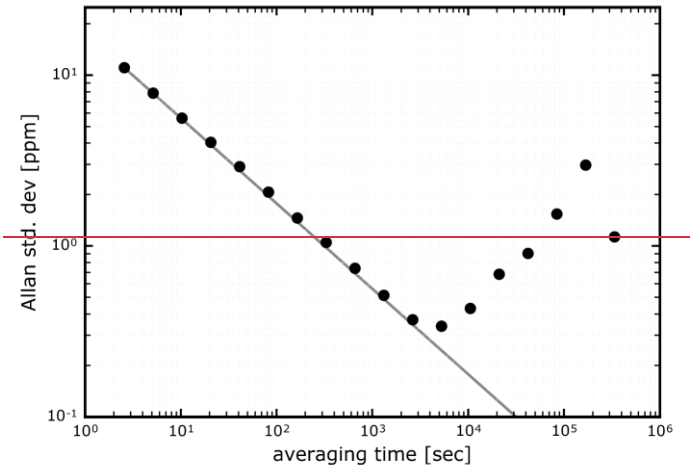

837

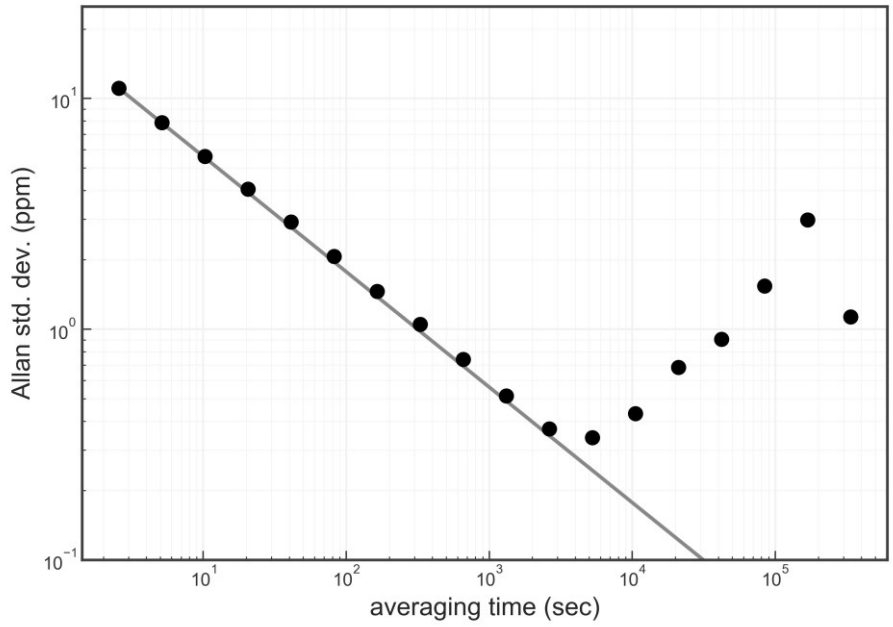

838

839 Figure 9. Precision of O_2 mole fraction measured from a tank of synthetic air. Filled circles

840 are measurements and the line shows the ideal $\tau^{-1/2}$ dependence.

841

842

843

844

845

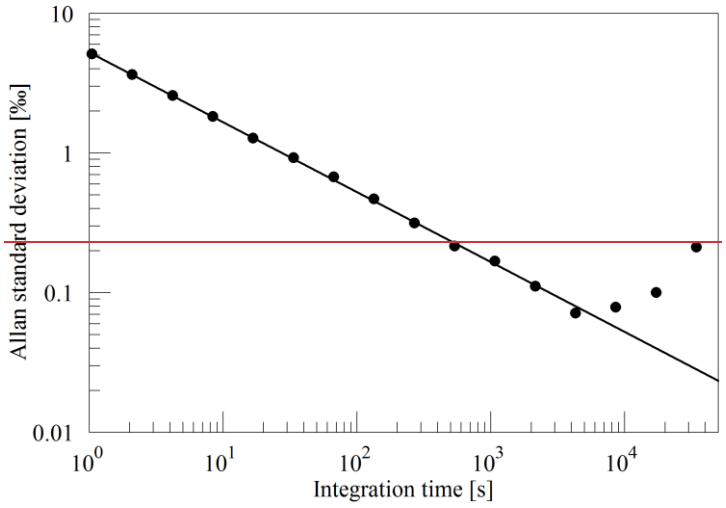

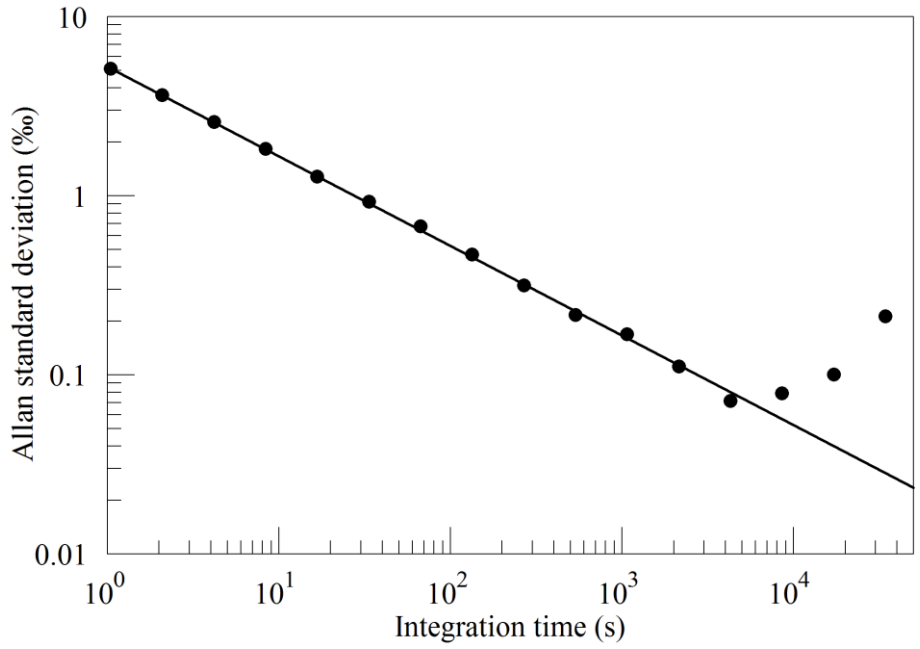

Figure 10. Precision of $\delta(^{18}O)$ measured from a tank of synthetic air. Filled circles are measurements and the line shows the ideal $\tau^{-1/2}$ dependence.

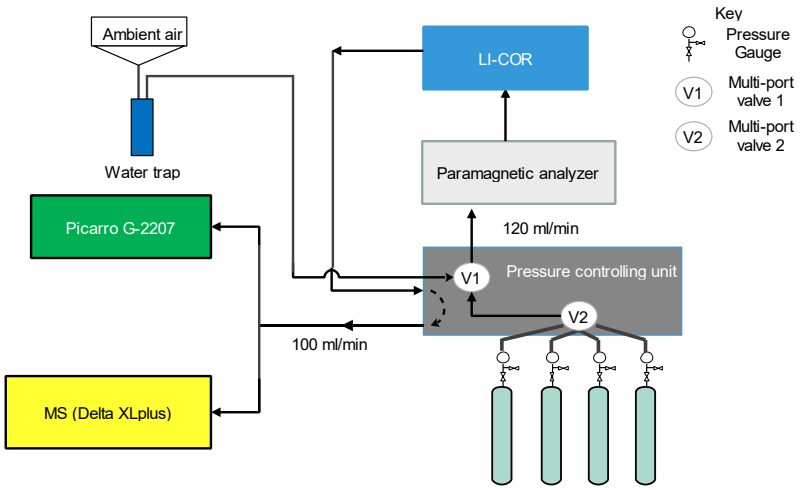

Figure 11. Schematics of the measurement system used to compare the Picarro analyzer with the Mass Spectrometer at Bern.

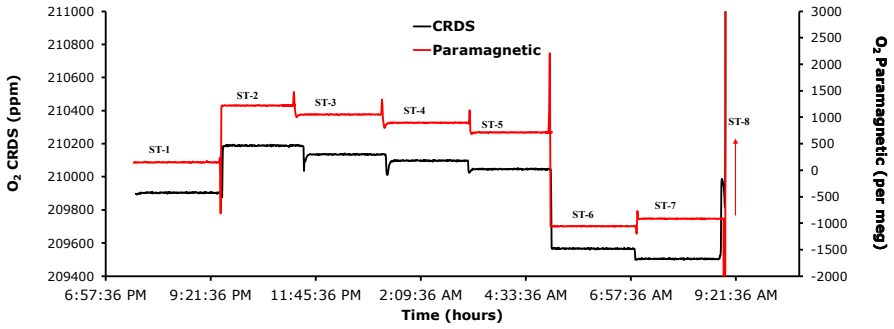

Figure 12. Comparison of oxygen mixing ratios for the seven standard gases measured using the CRDS analyzer (black) and the Paramagnetic sensors (red).

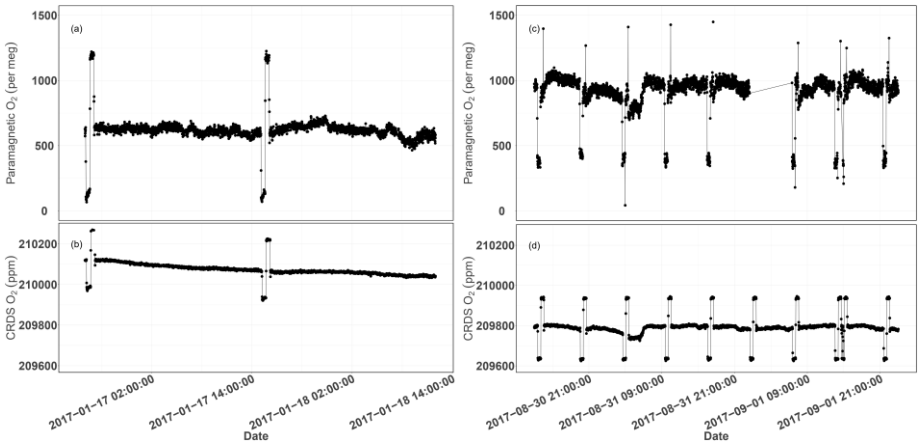

Figure 13. Parallel ambient air measurements by the Paramagnetic and CRDS analyzers at the beginning of the testing period (Panels a & b, January 2017) and the second phase of testing (Panels c & d, September 2017). The spikes are measurements from the two standard gases bracketing the ambient air values.

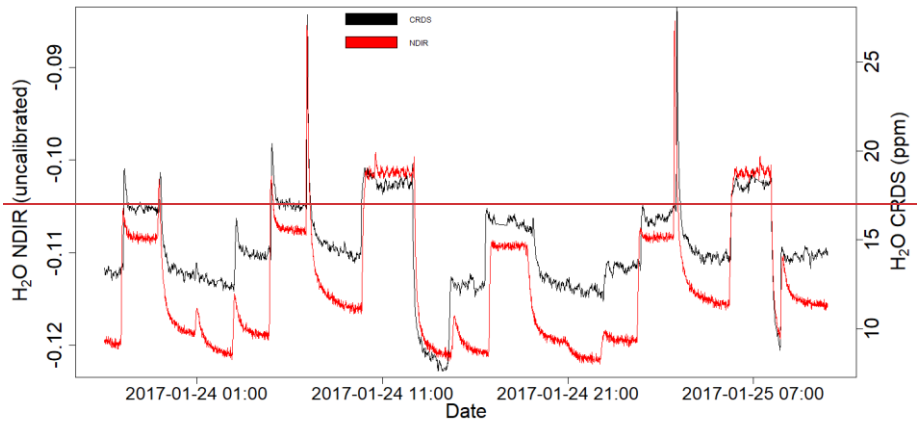
CRDS
NDIR
H2O NDIR (uncalibrated)
-0.09
-0.10
-0.11
-0.12
H2O CRDS (ppm)
25
20
15
10
2017-01-24 01:00
2017-01-24 11:00
2017-01-24 21:00
2017-01-25 07:00
Date

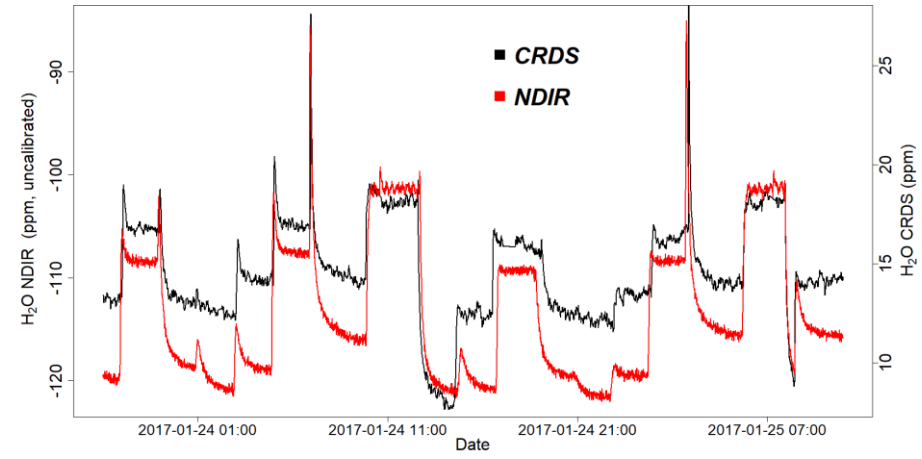
CRDS
NDIR
H2O NDIR (ppm, uncalibrated)
-90
-100
-110
-120
H2O CRDS (ppm)
25
20
15
10
2017-01-24 01:00
2017-01-24 11:00
2017-01-24 21:00
2017-01-25 07:00
Date

Figure 14. Parallel water vapor measurements for a dried ambient air by both the NDIR and CRDS analyzers. Note that the water values from the NDIR analyzer are not calibrated.

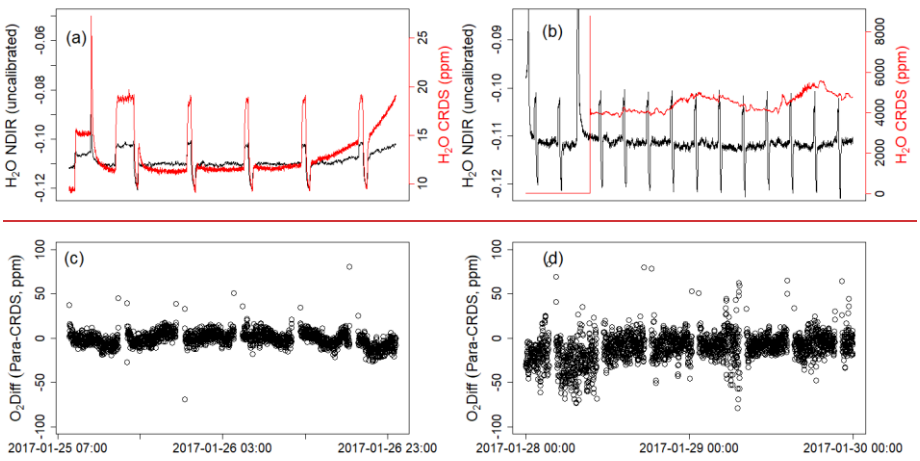

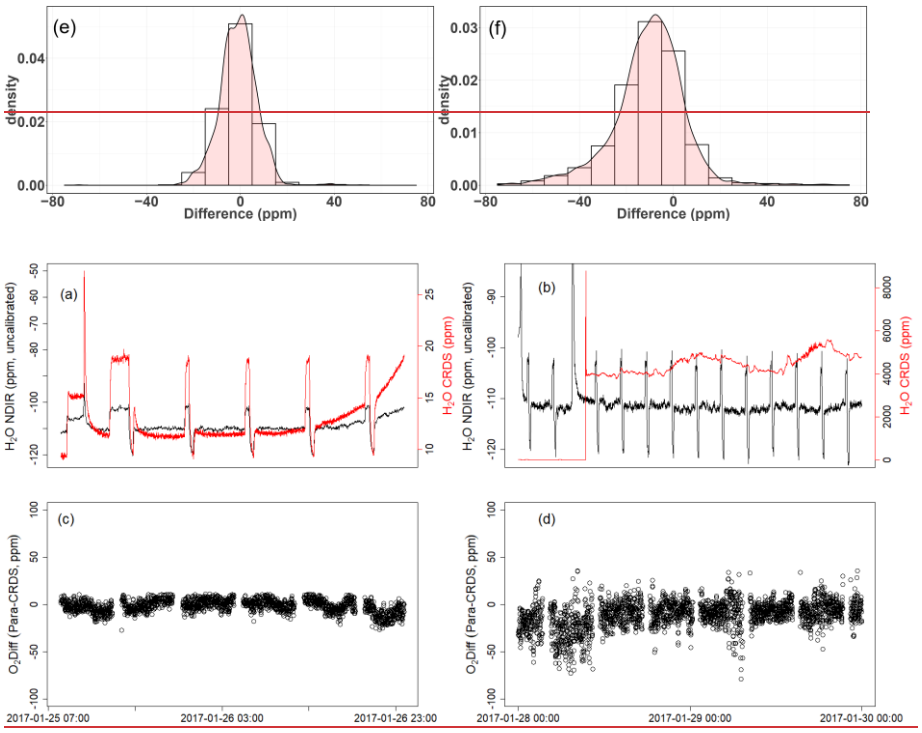
(e)
density
Difference (ppm)
(f)
density
Difference (ppm)
(a)
H2O NDIR (ppm, uncalibrated)
H2O CRDS (ppm)
(b)
H2O NDIR (ppm, uncalibrated)
H2O CRDS (ppm)
(c)
O2Diff (Para-CRDS, ppm)
2017-01-25 07:00
2017-01-26 03:00
2017-01-26 23:00
(d)
O2Diff (Para-CRDS, ppm)
2017-01-28 00:00
2017-01-29 00:00
2017-01-30 00:00

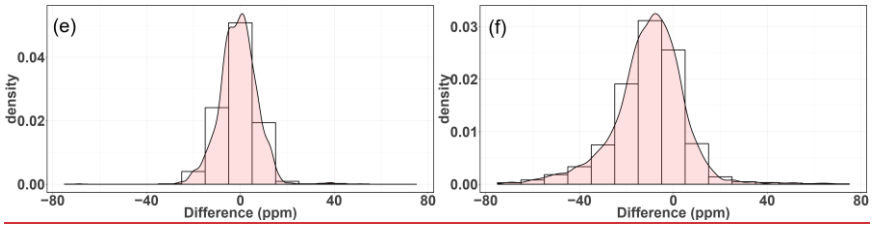
(e)
density
Difference (ppm)
(f)
density
Difference (ppm)

931

932 Figure 15. Results of water correction tests. Water measurements of the NDIR (left scale) for
933 dry conditions (a,b) and the CRDS analyzer (right scale) for dry (a) and wet (b) conditions.
934 The difference in oxygen measurements between the Paramagnetic and the CRDS instrument
935 using the built-in water correction for the CRDS values under dry (c) and wet (d) conditions.
936 Panels (e) and (f) show the population density functions.

937

938

939

940

941

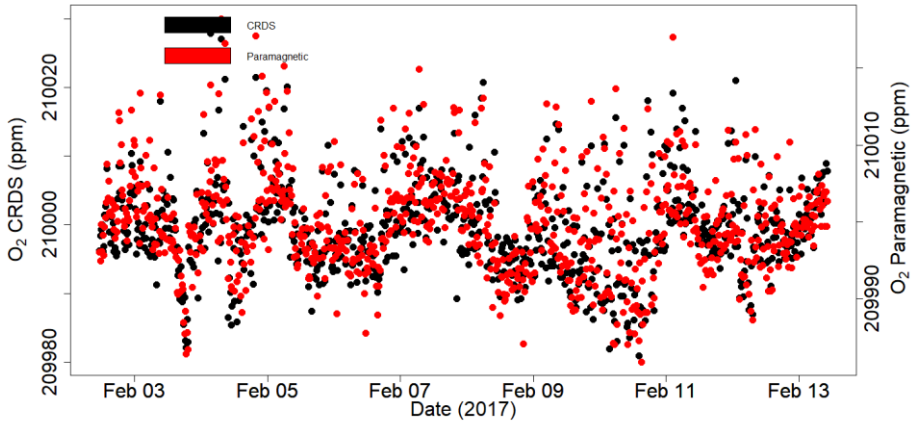

942

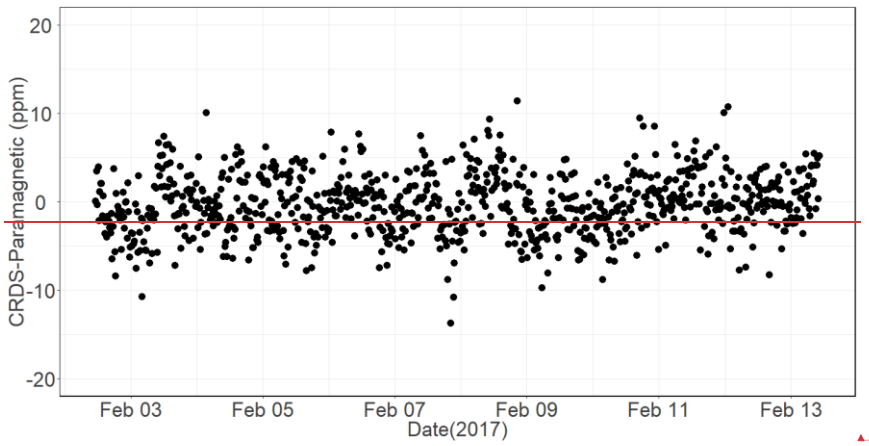

943

Formatted: English (United States)

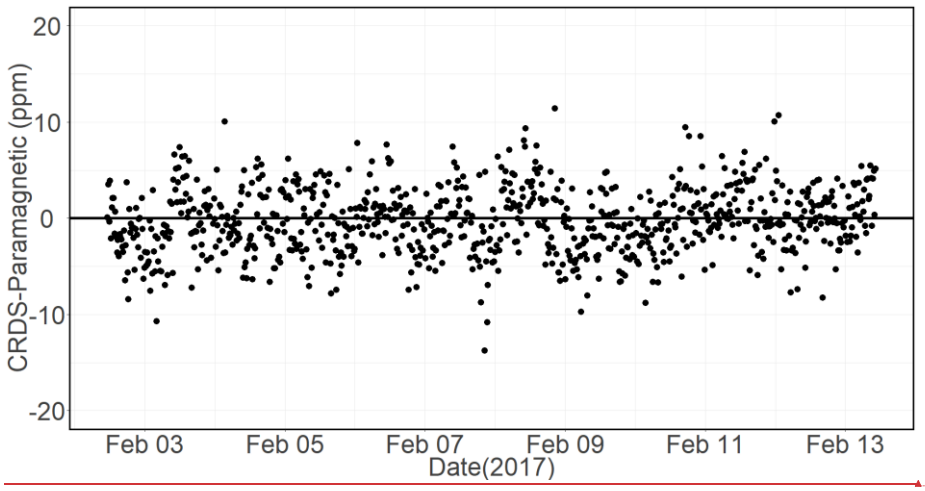

Figure 16. Calibrated ambient air oxygen measurements (1-minute average) at the Jungfraujoch site using the CRDS and Paramagnetic analyzers both in ppm units (a) and the absolute difference between the two measurements in ppm (b) by matching time stamps.

Formatted: English (United States)

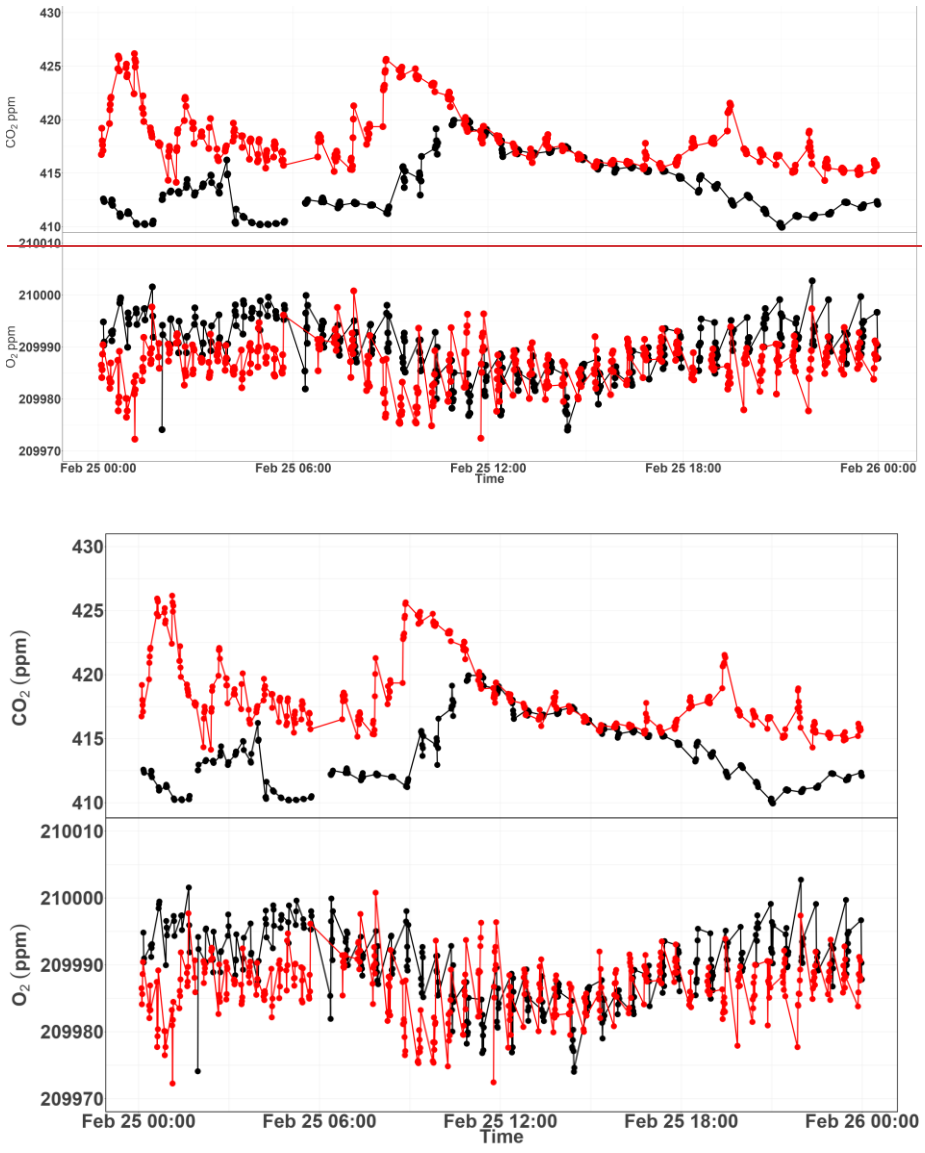

952

953

954 Figure 17. Diurnal variations of CO_2 (top) and O_2 (bottom) measurements from the 12 m (red)

955 and the 212.5 m (black) height levels at Beromünster tower.

956

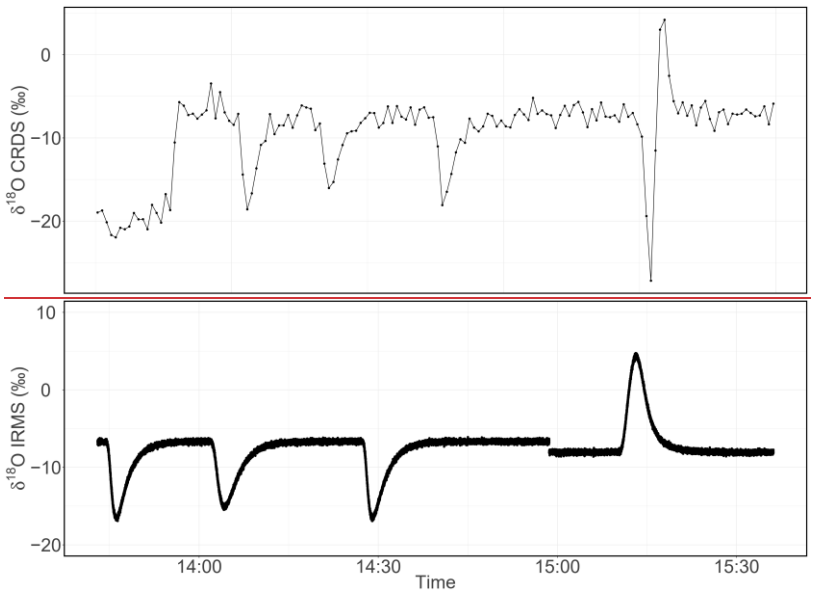
0
−10
−20
δ18O CRDS (‰)
10
0
−10
−20
δ18O IRMS (‰)
14:00
14:30
15:00
15:30
Time

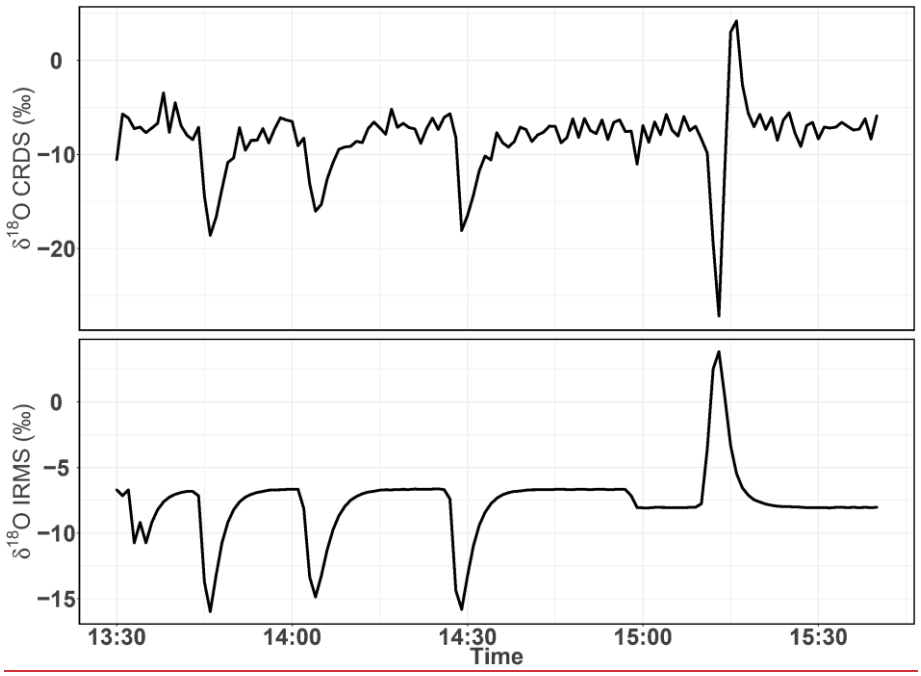

Figure 18. Consecutive $\delta^{18}O$ measurements of a standard gas (CO_2-free air) filled into three flasks followed by measurement of breath air using the CRDS analyzer (top) and IRMS (bottom). These measurements were carried out in the middle of ambient air measurements.

Appendix A.

~~Additional plots~~

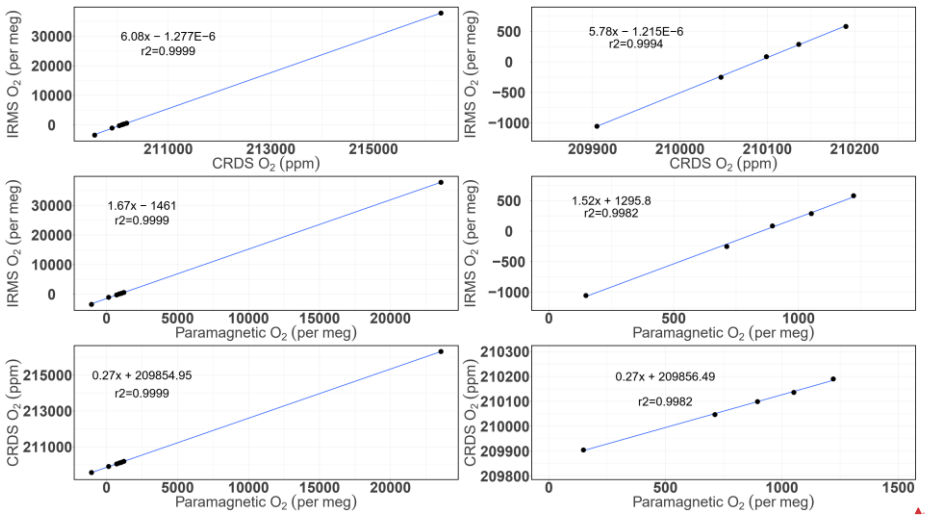

Figure A.1. Correlations between the O_2 mixing ratios measured by the CRDS and Paramagnetic analyzers with the mass spectrometric measurements (uncalibrated values). The left panels are for all the cylinders measured (standards 1 to 8) while the right ones are after ~~zooming only to~~selecting standards 1-5.

994

995 **References**

996 Battle, M., Bender, M. L., Tans, P. P., White, J. W. C., Ellis, J. T., Conway, T., and Francey, R. J.: Global
997 carbon sinks and their variability inferred from atmospheric O-2 and delta C-13, Science, 287, 2467-
998 2470, 2000.

999 Bender, M. L., Tans, P. P., Ellis, J. T., Orchardo, J., and Habfast, K.: A High-Precision Isotope Ratio
1000 Mass-Spectrometry Method for Measuring the O-2 N-2 Ratio of Air, Geochim Cosmochim Ac, 58,
1001 4751-4758, 1994.

1002 Berhanu, T. A., Satar, E., Schanda, R., Nyfeler, P., Moret, H., Brunner, D., Oney, B., and Leuenberger,
1003 M.: Measurements of greenhouse gases at Beromünster tall tower station in Switzerland, Atmos.
1004 Meas. Tech. , 9, 2016.

1005 Berhanu, T. A., Szidat, S., Brunner, D., Satar, E., Schanda, R., Nyfeler, P., Battaglia, M., Steinbacher,
1006 M., Hammer, S., and Leuenberger, M.: Estimation of the fossil-fuel component in atmospheric CO2
1007 based on radiocarbon measurements at the Beromünster tall tower, Switzerland, Atmos. Chem.
1008 Phys. Discuss., 2017, 1-33, 2017.

1009 Crosson, E. R. J. A. P. B.: A cavity ring-down analyzer for measuring atmospheric levels of methane,
1010 carbon dioxide, and water vapor, 92, 403-408, 2008.

1011 Filges, A., Gerbig, C., Rella, C. W., Hoffnagle, J., Smit, H., KrÃ¤mer, M., Spelten, N., Rolf, C., BozÃ³ki, Z.,
1012 Buchholz, B., and Ebert, V.: Evaluation of the IAGOS-Core GHG Package H2O measurements during
1013 the DENCHAR airborne inter-comparison campaign in 2011, Atmos. Meas. Tech., 11, 5279–5297,
1014 2018, https://doi.org/10.5194/amt-11-5279-2018. ~~Atmos. Meas. Tech. Discuss., doi: 10.5194/amt-~~
1015 ~~2018-36, 2018. 2018.~~

1016 ~~Fleisher, A. J., Hodges, J., and Sironneau, V.: Collision-dependent line areas in the a1Δg← X3Σ−g band~~
1017 ~~of molecular oxygen, 2015.~~

1018 Gao, F., Zhang, X., Zhang, X., Wang, M., and Wang, P.: Virtual electronic nose with diagnosis model
1019 for the detection of hydrogen and methane in breath from gastrointestinal bacteria, 28-31 May 2017
1020 2017, 1-3.
1021 Gordon, E., Rothman, S., Hill, C., Kochanov, V., Tan, Y., Bernath, P., Birk, M., Boudon, V., Campargue,
1022 A., Chance, K., Drouin, J., Flaud, J., Gamache, R. R., Hodges, J., Jacquemart, D., Perevalov, I., Perrin, A.,
1023 Shine, P., Smith, M., Tennyson, J., Toon, G., Tran, H., Tyuterev, G., Barbe, A., Császár, G., Devi, M.,
1024 Furtenbacher, T., Harrison, J., Hartmann, J., Jolly, A., Johnson, J., Karman, T., Kleiner, I., Kyuberis, A.
1025 A., Loos, J., Lyulin, M., Massie, S., Mikhailenko, S., Moazzen-Ahmadi, N., Muller, S., Naumenko, O. V.,
1026 Nikitin, A. V., Polyansky, O. L., Rey, M., Rotger, M., Sharpe, S., Sung, K., Starikova, E., Tashkun, S.,
1027 Auwera, J., Wagner, G., Wilzewski, J., Wcisło, P., Yu, S., and Zak, E. J.: The HITRAN2016 molecular
1028 spectroscopic database, 203, 3 - 69, 2017.
1029 Goto, D., Morimoto, S., Ishidoya, S., Aoki, S., and Nakazawa, T.: Terrestrial biospheric and oceanic
1030 CO2 uptake estimated from long-term measurements of atmospheric CO2 mole fraction, δ13C and
1031 δ(O2/N2) at Ny-Ålesund, Svalbard, Journal of Geophysical Research: Biogeosciences, doi:
1032 10.1002/2017JG003845, 2017. n/a-n/a, 2017.
1033 Gottlieb, K., Le, C. X., Wacher, V., Sliman, J., Cruz, C., Porter, T., and Carter, S.: Selection of a cut-off
1034 for high- and low-methane producers using a spot-methane breath test: results from a large north
1035 American dataset of hydrogen, methane and carbon dioxide measurements in breath, Gastroenterol
1036 Rep, 5, 193-199, 2017.
1037 Hartmann, J.-M., Boulet, C., and Robert, D.: Collisional Effects on Molecular Spectra, Elsevier Science,
1038 2008.
1039 Henne, S., Brunner, D., Folini, D., Solberg, S., Klausen, J., and Buchmann, B.: Assessment of
1040 parameters describing representativeness of air quality in-situ measurement sites, Atmos. Chem.
1041 Phys., 10, 3561-3581, 2010.

1042 Hodges, J. T., Layer, H. P., Miller, W. W., and Scace, G. E.: Frequency-stabilized single-mode cavity
1043 ring-down apparatus for high-resolution absorption spectroscopy, 75, 849-863, 2004.
1044 Keeling, R. F.: Development of an Interferometric Oxygen Analyzer for Precise Measurement of the
1045 Atmospheric O2 Mole Fraction, UMI, 1988a.
1046 Keeling, R. F.: Measuring correlations between atmospheric oxygen and carbon dioxide mole
1047 fractions: A preliminary study in urban air, J Atmos Chem, 7, 153-176, 1988b.
1048 Keeling, R. F. and Manning, A. C.: 5.15 - Studies of Recent Changes in Atmospheric O2 Content A2 -
1049 Holland, Heinrich D. In: Treatise on Geochemistry (Second Edition), Turekian, K. K. (Ed.), Elsevier,
1050 Oxford, 2014.
1051 Keeling, R. F. and Shertz, S. R.: Seasonal and Interannual Variations in Atmospheric Oxygen and
1052 Implications for the Global Carbon-Cycle, Nature, 358, 723-727, 1992.
1053 Keeling, R. F., Stephens, B. B., Najjar, R. G., Doney, S. C., Archer, D., and Heimann, M.: Seasonal
1054 variations in the atmospheric O-2/N-2 ratio in relation to the kinetics of air-sea gas exchange, Global
1055 Biogeochem Cy, 12, 141-163, 1998.
1056 Lamouroux, J., Sironneau, V., Hodges, J. T., and Hartmann, J. M.: Isolated line shapes of molecular
1057 oxygen: Requantized classical molecular dynamics calculations versus measurements, Physical
1058 Review A, 89, 042504, 2014.
1059 Le Quéré, C., Andrew, R. M., Friedlingstein, P., Sitch, S., Pongratz, J., Manning, A. C., Korsbakken, J. I.,
1060 Peters, G. P., Canadell, J. G., Jackson, R. B., Boden, T. A., Tans, P. P., Andrews, O. D., Arora, V. K.,
1061 Bakker, D. C. E., Barbero, L., Becker, M., Betts, R. A., Bopp, L., Chevallier, F., Chini, L. P., Ciais, P.,
1062 Cosca, C. E., Cross, J., Currie, K., Gasser, T., Harris, I., Hauck, J., Haverd, V., Houghton, R. A., Hunt, C.
1063 W., Hurtt, G., Ilyina, T., Jain, A. K., Kato, E., Kautz, M., Keeling, R. F., Klein Goldewijk, K., Körtzinger, A.,
1064 Landschützer, P., Lefèvre, N., Lenton, A., Lienert, S., Lima, I., Lombardozzi, D., Metzl, N., Millero, F.,
1065 Monteiro, P. M. S., Munro, D. R., Nabel, J. E. M. S., Nakaoka, S. I., Nojiri, Y., Padín, X. A., Peregon, A.,
1066 Pfeil, B., Pierrot, D., Poulter, B., Rehder, G., Reimer, J., Rödenbeck, C., Schwinger, J., Séférian, R.,

1067 Skjelvan, I., Stocker, B. D., Tian, H., Tilbrook, B., van der Laan-Luijkx, I. T., van der Werf, G. R., van
1068 Heuven, S., Viovy, N., Vuichard, N., Walker, A. P., Watson, A. J., Wiltshire, A. J., Zaehle, S., and Zhu,
1069 D.: Global Carbon Budget 2017, Earth Syst. Sci. Data Discuss., 2017, 1-79, 2017.
1070 Manning, A.: Temporal variability of atmospheric oxygen from both continuos and measurements
1071 and a flask sampling network: tools for studying the global carbon cycle, Ph.D. Ph.D., University of
1072 California, San Diego, San Diego, Calofornia, USA, 2001.
1073 Manning, A. C. and Keeling, R. F.: Global oceanic and land biotic carbon sinks from the Scripps
1074 atmospheric oxygen flask sampling network, Tellus B, 58, 95-116, 2006.
1075 Manning, A. C., Keeling, R. F., and Severinghaus, J. P.: Precise atmospheric oxygen measurements
1076 with a paramagnetic oxygen analyzer, Global Biogeochem Cy, 13, 1107-1115, 1999.
1077 Marrero, T. R. and Mason, E. A.: Gaseous Diffusion Coefficients, Journal of Physical and Chemical
1078 Reference Data 1, 3, 1972.
1079 Martin, N. A., Ferracci, V., Cassidy, N., and Hoffnagle, J. A. J. A. P. B.: The application of a cavity ring-
1080 down spectrometer to measurements of ambient ammonia using traceable primary standard gas
1081 mixtures, 122, 219, 2016.
1082 Mckay, L. F., Eastwood, M. A., and Brydon, W. G.: Methane Excretion in Man - a Study of Breath,
1083 Flatus, and Feces, Gut, 26, 69-74, 1985.
1084 Nevison, C. D., Keeling, R. F., Kahru, M., Manizza, M., Mitchell, B. G., and Cassar, N.: Estimating net
1085 community production in the Southern Ocean based on atmospheric potential oxygen and satellite
1086 ocean color data, Global Biogeochem Cy, 26, 2012.
1087 Oney, B., Henne, S., Gruber, N., Leuenberger, M., Bamberger, I., Eugster, W., and Brunner, D.: The
1088 CarboCount CH sites: characterization of a dense greenhouse gas observation network, Atmos.
1089 Chem. Phys., 15, 11147-11164, 2015.
1090 Press, W. H., Teukolsky, S. A., Vetterling, W. T., and Flannery, B. P.: Numerical Recipes 3rd Edition:
1091 The Art of Scientific Computing, Cambridge Printing Press, Cambridge, England, 1986.

Press, W. H., Teukolsky, S. A., Vetterling, W. T., and Flannery, B. P.: Numerical recipes in C: the art of scientific computing, Cambridge University Press, London, 1992.

~~Rothman, L. S., Gordon, I. E., Babikov, Y., Barbe, A., Chris Benner, D., Bernath, P. F., Birk, M., Bizzocchi, L., Boudon, V., Brown, L. R., Campargue, A., Chance, K., Cohen, E. A., Coudert, L. H., Devi, V. M., Drouin, B. J., Fayt, A., Flaud, J. M., Gamache, R. R., Harrison, J. J., Hartmann, J. M., Hill, C., Hodges, J. T., Jacquemart, D., Jolly, A., Lamouroux, J., Le Roy, R. J., Li, G., Long, D. A., Lyulin, O. M., Mackie, C. J., Massie, S. T., Mikhailenko, S., Müller, H. S. P., Naumenko, O. V., Nikitin, A. V., Orphal, J., Perevalov, V., Perrin, A., Polovtseva, E. R., Richard, C., Smith, M. A. H., Starikova, E., Sung, K., Tashkun, S., Tennyson, J., Toon, G. C., Tyuterev, V. G., and Wagner, G.: The HITRAN2012 molecular spectroscopic database, Journal of Quantitative Spectroscopy and Radiative Transfer, 130, 4-50, 2013.~~

Ryter, S. W. and Choi, A. M. K.: Carbon monoxide in exhaled breath testing and therapeutics, J Breath Res, 7, 2013.

Satar, E., Berhanu, T. A., Brunner, D., Henne, S., and Leuenberger, M.: Continuous CO2/CH4/CO measurements (2012–2014) at Beromünster tall tower station in Switzerland, Biogeosciences, 13, 2623-2635, 2016.

Schibig, M. F., Steinbacher, M., Buchmann, B., van der Laan-Luijkx, I. T., van der Laan, S., Ranjan, S. and Leuenberger, M. C,: Comparison of continuous in situ CO2 observations at Jungfraujoch using two different measurement techniques, Atmospheric Measurement Techniques , 8, 57-68, 10.5194/amt-8-57-2015, 2015.

Severinghaus, J. P.: Studies of the terresterial O2 and carbon cycles in sand dune gases and in Biosphere Doctoral Ph.D., Columbia University, New York, USA, 1995.

Steig, E. J., Gkinis, V., Schauer, A. J., Schoenemann, S. W., Samek, K., Hoffnagle, J., Dennis, K. J., and Tan, S. M.: Calibrated high-precision ¹⁷O-excess measurements using cavity ring-down spectroscopy with laser-current-tuned cavity resonance, Atmos. Meas. Tech., 7, 2014.

Stephens, B. B., Bakwin, P. S., Tans, P. P., Teclaw, R. M., and Baumann, D. D.: Application of a differential fuel-cell analyzer for measuring atmospheric oxygen variations, J Atmos Ocean Tech, 24, 82-94, 2007.

Sturm, P., M. Leuenberger, F.L. Valentino, B. Lehmann, and B. Ihly, Measurements of CO_2, its stable isotopes, O_2/N_2, and ^{222}Rn at Bern, Switzerland, *Atmospheric Chemistry and Physics*, *6*, 1991-2004, 2006.

Tennyson, J., Bernath, P. F., Campargue, A., Császár, A. G., Daumont, L., Gamache, R. R., Hodges, J. T., Lisak, D., Naumenko, O. V., Rothman, L. S., Tran, H., Zobov, N. F., Buldyreva, J., Boone, C. D., De Vizia, M. D., Gianfrani, L., Hartmann, J.-M., McPheat, R., Weidmann, D., Murray, J., Ngo, N. H., and Polyansky, O. L.: Recommended isolated-line profile for representing high-resolution spectroscopic transitions (IUPAC Technical Report), 86, 1931–1943, 2014.

Tohjima, Y.: Method for measuring changes in the atmospheric O-2/N-2 ratio by a gas chromatograph equipped with a thermal conductivity detector, J Geophys Res-Atmos, 105, 14575-14584, 2000.

Tran, H., Turbet, M., Hanoufa, S., Landsheere, X., Chelin, P., Ma, Q., Hartmann, J.: The CO2–broadened H2O continuum in the 100–1500 cm-1 region: Measurements, predictions and empirical model, Journal of Quantitative Spectroscopy and Radiative Transfer, 230, 75-80, 2019.

Valentino, F. L., Leuenberger, M., Uglietti, C., and Sturm, P.: Measurements and trend analysis of O2, CO2 and δ13C of CO2 from the high altitude research station Junfgraujoch, Switzerland — A comparison with the observations from the remote site Puy de Dôme, France, Sci Total Environ, 391, 203-210, 2008.

Varghese, P. L. and Hanson, R. K.: Collisional narrowing effects on spectral line shapes measured at high resolution, Appl. Opt., 23, 2376-2385, 1984.

1140 Wójtewicz, S., Cygan, A., Masłowski, P., Domysławska, J., Wcisło, P., Zaborowski, M., Lisak, D.,
1141 Trawiński, R. S., and Ciuryło, R.: Spectral line-shapes of oxygen B-band transitions measured with
1142 cavity ring-down spectroscopy, Journal of Physics: Conference Series, 548, 012028, 2014.
1143 Wolf, P. G., Parthasarathy, G., Chen, J., O'Connor, H. M., Chia, N., Bharucha, A. E., and Gaskins, H. R.:
1144 Assessing the colonic microbiome, hydrogenogenic and hydrogenotrophic genes, transit and breath
1145 methane in constipation, Neurogastroent Motil, 29, 2017.
1146 Zellweger, C., Forrer, J., Hofer, P., Nyeki, S., Schwarzenbach, B., Weingartner, E., Ammann, M., and
1147 Baltensperger, U.: Partitioning of reactive nitrogen (NO_y) and dependence on
1148 meteorological conditions in the lower free troposphere, Atmos. Chem. Phys., 3, 779-796, 2003.

1149